

## Sequential kinetics of a muscovite-out reaction: A natural example

ANTONIO SANCHEZ-NAVAS

Departamento de Mineralogía y Petrología—Instituto Andaluz de Ciencias de la Tierra, Universidad de Granada, C.S.I.C. 18071 Granada, Spain

### ABSTRACT

A natural example of sequential kinetics for the muscovite dehydration reaction in highly deformed mylonitic gneisses is analyzed. Studied textures consist of deformed pegmatitic muscovite crystals surrounded by fibrolitic sillimanite tightly intergrown with biotite and with potassium feldspar in the pressure shadows. Potassium feldspar, andalusite, biotite, and quartz appearing in the crystal core constitute the products of muscovite breakdown produced by topotactic replacement of muscovite within a single crystal. Non-isochemical decomposition of muscovite is proposed in which diffusion of  $K^+$  outward from the crystal took place along the muscovite interlayer and shear planes parallel to (001). The chemical potential gradient calculated for  $K$  capable of producing the texture observed within the pegmatitic crystals, results not only from the overstepping of the muscovite-out reaction but also from the difference in free energy between andalusite and sillimanite under  $P$ - $T$  conditions where andalusite is stable. The overall reaction within the andalusite stability field consists of the transformation  $1 Ms + 1 Qtz \rightarrow 1 And + 1 Kfs + 1 H_2O$  and of the indirect replacement  $0.25 Sil \rightarrow 0.25 And$ . Andalusite nucleation and growth took place completely inside muscovite, whereas most of the potassium feldspar was produced outside, preferentially at pressure shadows, after outward intracrystalline diffusion of  $K^+$  and fibrolitic sillimanite dissolution in the matrix. The rate-limiting step of this reaction process was initially the migration rate of the muscovite-andalusite and muscovite-potassium feldspar interfaces. However, it was followed by a diffusion-controlled step. The change in the relative rates of the reaction mechanisms was due to the coarsening of the reaction products, the low amount of energy and time required for non-reconstructive transformations (periodic bond chains of the tetrahedral sheet of muscovite are inherited by potassium feldspar and those of the octahedral sheet by andalusite), the magnitude of the heat flow associated with a possible contact metamorphic episode, and the slow diffusion of  $K^+$  within the crystal. Intracrystalline diffusion took place through a double monolayer of adsorbed molecules of water ( $\sim 10 \text{ \AA}$ ) localized at microcleavages produced by basal slip in the interlayer level, instead of a proper lattice diffusion process. The derived rate law at constant  $P$  and  $T$  (considering the cases of 2 kbar and 605 °C and 3 kbar and 639 °C) for the diffusion-controlled process gives a time span of about 10 000 years for the growth of these metamorphic textures, which seems to be a reasonable estimate for a contact metamorphic event.

### INTRODUCTION

The rate of a mineral reaction is determined by the rate of the slowest one of the following processes: (1) dissolution of reactant phases; (2) diffusion of chemical components from dissolved areas to those where the new minerals precipitate; (3) nucleation and growth of products; and (4) changes in temperature and pressure that produce the free-energy driving force. However, the first three rate-controlling steps are generally considered the only kinetic processes responsible for the preservation of minerals outside their stability fields when rocks passed along the  $P$ - $T$ - $t$  path of regional metamorphism. This is due to the generalized assumption that the rates of change for temperature and pressure associated with this kind of metamorphism

are so slow that the reactions remain close to equilibrium (Thompson and England 1984). Extensive disequilibrium can occur for reactions with very small entropy changes, such as the andalusite to sillimanite transformation. The effect of the large enthalpy (entropy) changes of the devolatilization reactions on the overstepping required to allow nucleation and growth of the reaction products, and on the rock temperatures has been evaluated by Ridley and Thompson (1986) and Ridley (1985). Walther and Wood (1984) have demonstrated that for dehydration reactions, with entropy changes of 20 cal/mol/°C at 500 °C and only 1 °C of overstep, the reaction proceeds to completion quite rapidly (<1000 y) when the dissolution rate of the reactants is the rate-controlling step. Schramke et al. (1987) experimentally obtained complete transformation of muscovite plus quartz to andalusite and potassium feldspar, under low-pressure prograde metamorphism, close to the equilibrium boundary, with the rate-controlling surface area being that of the growing andalusite.

\* E-mail: asnavas@goliat.ugr.es

Lasaga (1986) analyzed the role of diffusion and surface reactions in the kinetics of dehydration of muscovite plus quartz. He demonstrated that, for normal values of diffusion coefficients of the species in the intergranular fluid and porosity and tortuosity of rocks, andalusite surface kinetics control the reaction rate both under experimental conditions and in natural situations. Only high-temperature oversteps and diffusion distances may produce control by diffusion transport for the muscovite-out reaction (see his Fig. 6). He also demonstrated the importance of using a non-linear rate law for this reaction, to explain both small and large deviations from equilibrium. This would contradict the assertions of Fisher (1978) in relation to sequential kinetics in the development of metamorphic structures, where he holds that an initial reaction-controlled stage will end long before the structure is large enough to detect, because it is based on the assumption that there is a linear relation between chemical reaction rates and reaction affinity. Moreover, Kerrick et al. (1991), on the basis of experimental studies, considered the reactions rates at the surface area of solids as the rate-limiting process for typical heterogeneous reactions involving fluids. However, many metamorphic processes involve diffusion-controlled mineral growth (Fisher 1970; Joesten 1977; Foster 1981, 1983, 1986). Their development is favored by high heat flow, such as in contact aureoles, and by the inhibition of diffusion due to the absence of water in the grain boundary network, such as occurs in retrogressively and/or statically metamorphosed rocks.

Brearely (1986) and Worden et al. (1987) have shown that the muscovite structure controls the crystallization of the products of the breakdown reaction in natural samples during pyrometamorphism. Muscovite pseudomorphs are in structural continuity with the precursor single crystal, such that they have grown with their close-packed planes [(001) biotite, (010) sanidine, for example] parallel to the (001) plane of the phengites (the plane of closest oxygen packing). These crystallographic relationships have also been observed in experiments on muscovite breakdown under similar conditions of marked overstepping temperatures (Rubie and Brearely 1987; Brearely and Rubie 1990).

Fisher (1978) showed that after nucleation of stable new minerals in a rock, the growth of the resulting metamorphic structures goes through a definite sequence of stages, in which the mechanism that determines the overall rate of mineral growth for each stage, the rate-controlling step, depends on local and regional changes in variables such as the distance between the initial nuclei, grain size, diffusion coefficients, and heat flow rates.

This paper examines a natural example of sequential kinetics for the muscovite dehydration reaction in ductile deformed mylonitic gneisses. The textures that were studied are similar to some presented by García-Casco et al. (1993), and they consist of deformed pegmatitic muscovite crystals surrounded by fibrolitic sillimanite tightly intergrown with biotite, with potassium feldspar in the pressure shadows, and with andalusite, potassium feldspar, biotite, and quartz in the crystal core. The crystallographic relations established for the phases involved indicate the existence of topotactic replacement of muscovite by potassium feldspar and andalusite in the cores. Deduced

reaction mechanisms have allowed to calculate the overall reaction and to determine the sequence of stages these metamorphic structures have undergone: (1) An initial interface-controlled stage; (2) an intermediate intracrystalline diffusion-controlled stage; and (3) a probable final heat-flow-controlled stage for the muscovite breakdown reaction process.

### ANALYTICAL PROCEDURES

An automated CAMECA SX50 electron microprobe (Centro de Investigación Científica at the University of Granada) was used to obtain backscattered electron (BSE) and X-ray images on areas smaller than approximately  $100 \times 100 \mu\text{m}$ . Electronic images of larger zones were obtained by moving the sample in a square-shaped area while using a position-fixed beam. The beam spot size, the step-to-step displacement and the acquisition time were optimized to obtain good analytical and spatial resolution. Modal analyses were performed on diverse BSE and X-ray images by image-analysis processes, using a color palette in isocountour and segmentation mode to obtain precise quantification of the mineral areas.

Samples for TEM study were prepared as Canadian Balsam-mounted thin sections oriented approximately normal to (001) crystallographic planes of the pegmatitic muscovite single crystals and to the *c* axis of the andalusite prisms inside them. Samples were further thinned using a Gatan 600 ion mill and then carbon-coated for TEM observation with a PHILIPS CM-20 scanning transmission electron microscope (STEM) operated at 200 kV and equipped with an EDAX solid-state energy-dispersive X-ray detector (EDX). An objective aperture of  $40 \mu\text{m}$  was used to obtain a compromise between amplitude and phase contrast for the images, so reflections with *d*-values  $> 0.4 \text{ nm}$  were used for the lattice-fringe images.

### GEOLOGICAL SETTING AND SAMPLE DESCRIPTION

Together with the Rifian Cordilleras, the Betic Cordilleras constitute the westernmost part of the Alpine Mediterranean Orogen. The Internal Zones of the Betic Cordilleras comprise the Nevado-Filabride, the Alpujarride and the Malaguide nappe complexes, in ascending tectonic order. Within the western (or upper) Alpujarrides, two main groups of units can be distinguished: the upper Casares-Los Reales Group and the lower Blanca Group (Martín-Algarra 1987). The base of the Los Reales nappes consists of peridotites, mainly lherzolites, with minor dunites and harzburgites (Obata 1980). The Los Reales unit overlies the Blanca unit of the Alpujarride Complex (Mollat 1968); the contact was originally a compressional thrust but is now an extensional low-angle normal fault (García Dueñas and Balanyá 1991). Torres-Roldán (1974, 1979, 1981) established two different *P-T* gradients during metamorphism of the Casares-Los Reales type units: an earlier medium-slope gradient ( $27 \text{ }^\circ\text{C}/\text{km}$ ) and a later one with much shallower slope ( $60 \text{ }^\circ\text{C}/\text{km}$ ). The change in physical conditions that caused the overprinting of the low *P-T* set of assemblages on the intermediate *P-T* ones was preceded by an episode of penetrative deformation that produced the megascopic or main foliation ( $D_2$  of Torres-Roldán 1981; and Cuevas et al. 1989). The *P-T* evolution of these rocks from the earlier intermediate-*P* conditions

to the later low-*P* ones included an intermediate stage of isothermal decompression (Torres-Roldán 1981).

The samples studied come from the lower part of the Torrox and Jubrique units belonging to the Los Reales type tectonic unit, but are located above the peridotites. Specifically, the samples are from muscovite-biotite-garnet banded gneisses and pegmatitic rocks of the Torrox orthogneiss complex [TGC; see Fig. 1 in García-Casco et al. (1993) for a geological sketch map of the Betic Cordilleras and the location of the TGC] and from pelitic gneisses in the Ronda peridotite aureole, located at the potassium feldspar isograd of the Gneiss Series of Loomis (1972a; see his Fig. 1 for the geological map, and his Fig. 2 for the location of the isograds). Although the gneisses constitute different structural units, both have been affected by the same geotectonic processes (Torres-Roldán 1974). The prekinematic minerals of the main foliation, termed  $S_2$ , in the pelitic rocks from the TGC and Ronda aureole are Ms, St, Grt, Ky, and Rt. The syn- $S_2$  minerals are Sil (fibrolitic), Bt, and Ilm, and the post- $S_2$  minerals are And, Bt, and Ilm [mineral abbreviations after Kretz (1983)]. The three  $Al_2SiO_5$  polymorphs appear in these high-grade rocks from the Los Reales type unit. The studied textures appear in pegmatitic muscovite crystals of banded gneisses and pegmatites from the TGC gneisses, and in muscovite pseudomorphs of quartz pods in the pelitic gneisses from the peridotite aureole. The andalusite-sillimanite transformation and the muscovite breakdown reaction observed in these samples were studied by Loomis (1972a) and García-Casco et al. (1993), although they interpreted the intersection of the dehydration reaction very differently. Prograde metamorphism (near isobaric heating) was proposed by Loomis (Fig. 10 in Loomis 1972a), whereas García-Casco et al. considered the muscovite-out reaction to be crossed during near-isothermal decompression (see their Fig. 11A for the proposed *P-T* path).

## RESULTS

### Muscovite breakdown textures

Muscovite breakdown textures studied in detail in this paper correspond to those observed in the pegmatitic muscovite crystals from muscovite-biotite-garnet banded gneisses of the TGC. The textures consist of deformed pegmatite muscovite crystals surrounded by fibrolitic sillimanite tightly intergrown with biotite, and with potassium feldspar in the pressure shadows (Fig. 1). Potassium feldspar, andalusite, and biotite appear in the crystal core (Figs. 1A, 1C, 2, 3A, 3B, and 3C). Particularly noteworthy is the existence of quartz as a reaction product of muscovite breakdown in the core of the muscovite crystals. Quartz is observed both in those textures in which the reaction products of these cores reach the matrix (Fig. 1C) and in those structures that appear clearly isolated from the matrix (Figs. 2 and 3A). Both andalusite and potassium feldspar form single crystals in the structures completely isolated from the matrix, with potassium feldspar adjacent to muscovite and andalusite in the inner part (Figs. 2 and 3A). Where these structures have reached the matrix, andalusite single crystals appear surrounded by a polycrystalline aggregate of andalusite, minor quantities of potassium feldspar are observed, and biotite crystals cover the internal muscovite boundary (Figs. 3B and 3C).

Ilmenite also appears intergrown with andalusite, potassium feldspar, biotite, and quartz (Fig. 1C).

Modal analyses performed on BSE and X-ray images of less-developed textures (Figs. 2B, 2C, and 3A) show molar proportions of 5:2:1 for andalusite, potassium feldspar, and quartz, respectively. In coarsened textures, the proportion changes to 3:1:1 (as in the case of the texture in Fig. 2D). Where it reaches the matrix, potassium feldspar decreases drastically in amount and is located only in cleavages along the muscovite basal planes, as occurs for the texture shown in Figure 1C, and specially the one in Figure 3C.

Reaction products of celadonic muscovite decomposition (Massonne and Schreyer 1987) such as biotite and quartz, appear extensively at the rims of pegmatitic muscovite crystals (Figs. 3B and 3D). This reaction has been studied by García-Casco et al. (1993) for matrix muscovites in these rocks. Cores of pegmatitic muscovite crystals where the breakdown reaction products occur are non-celadonic in contrast to the highly phengitic character of the rims.

Optical studies performed on the texture shown in Figure 3A, and on a basal plate fragment of the muscovite seen in Figure 1A (adjacent to the andalusite prisms) indicates that the *c* axis of andalusite coincides approximately with  $\langle 110 \rangle$  of the host pegmatitic muscovite. Fibrolitic sillimanite at the muscovite boundary (Figs. 1C and 1D), as well as that located in other shear planes of the matrix foliation and even within muscovite pseudomorphs (Fig. 1B), appears tightly intergrown with and growing from biotite, and should not be considered a product of muscovite breakdown. As shown in Figure 1D, a coarsening and/or coalescence process produced a prismatic sillimanite crystal from a precursor aggregate of fibrolite needle-like crystals [see Fig. 10 of Vernon (1987a) for a similar case of preferential coarsening of sillimanite fibers].

The muscovite-out reaction has also been studied in muscovite single crystals from pegmatitic bands from the TGC. In these bands the breakdown takes place in very slightly or non-deformed muscovite crystals through reaction with the adjacent matrix quartz. Reaction products, comprising potassium feldspar, andalusite, and biotite, replace muscovite crystals from the outer rim inward. No fibrolite is observed in these samples. In Figure 4A, an andalusite single crystal forms a pseudomorph after muscovite in a pressure shadow on a pegmatitic tourmaline, preserving even its cleavage. The existence in some cases of alternating bands of andalusite and potassium feldspar in certain replacement structures is also noted (Fig. 4B). Modal analyses reveal approximately equal molar proportions of potassium feldspar and andalusite, although migration of potassium feldspar has been observed in some cases.

In the pelitic gneisses of the Ronda peridotite aureole, muscovite breakdown is complete, and former muscovite crystals have been replaced topotactically by andalusite, potassium feldspar, and biotite (Fig. 5A). Within pseudomorphs, elongated sillimanite prisms and fibrolite have grown from biotite crystals following muscovite breakdown (Fig. 5).

### TEM study

Crystallographic relations observed optically between muscovite host and andalusite crystals have been confirmed by se-

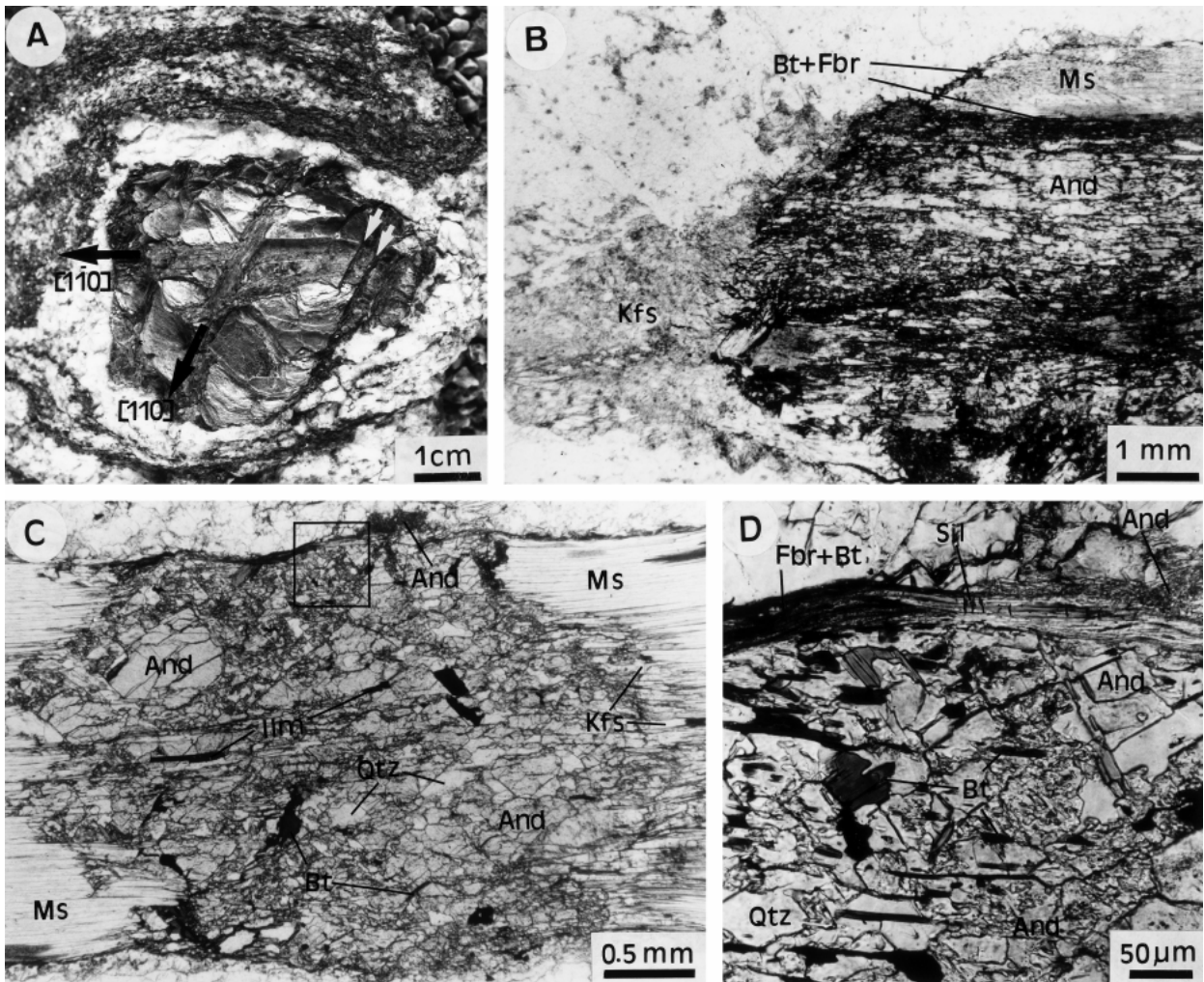


**FIGURE 1.** Textures of the muscovite breakdown reaction in banded gneisses from the TGC. **(A)** Outcrop photo of a deformed muscovite porphyroblast from banded gneisses with asymmetric pressure shadows indicating a dextral shear. Deformation produced kinking and fractures at kink boundaries, as well as subsidiary shear planes cutting mica layers, possibly generated through a domino bookshelf (arrows) and a carddeck mechanism (Price and Cosgrove 1990). Andalusite prisms occur along the  $[110]$  and  $[\bar{1}\bar{1}0]$  directions within these fracture planes. Potassium feldspar is located in the pressure shadows defined by the white areas adjacent to the muscovite single crystal. **(B)** Optical photomicrograph of a portion of a muscovite porphyroblast of banded gneisses pseudomorphed by andalusite with intergrown biotite and quartz. Potassium feldspar occurs within asymmetric pressure shadows and in very low quantities in some boundary zones between the relict muscovite and the replacing andalusite. Fibrolite appears tightly intergrown with biotite around the muscovite crystal and at shear planes that developed at the muscovite-andalusite boundary and within replacing andalusite. **(C)** Optical photomicrograph of an andalusite + quartz + biotite + potassium feldspar + ilmenite core within muscovite that has reached the matrix after coarsening. **(D)** A detail of (C) showing a prismatic sillimanite crystal tightly intergrown with biotite that has grown from an aggregate of fibrolite needlelike crystals.

lected-area electron diffraction (SAED) study of the muscovite-andalusite boundaries. The andalusite  $c$  axis approximately coincides with  $\langle 110 \rangle$  (or  $[010]$ ) of the muscovite (Fig. 6A). The transmission electron micrograph in Figure 6B, corresponding to this electron diffraction pattern, shows the presence of a grain boundary between the two phases, resulting in a non-coherent interface. However, muscovite relicts inside andalusite show the persistence, in spite of the crystal sizes, of a coherent interface with an approximate length of 65 nm across muscovite basal layers (Fig. 7A). Moiré fringe spacings of 1.5–2.2

nm have been found at semicoherent interfaces between muscovite and andalusite (Fig. 7B). Large areas without lattice fringes adjacent to this interface indicate significant elastic strain of the two lattices, producing disorientation in the vicinity of the interface. Transitions from grain boundaries to coherent or semicoherent interfaces occur throughout highly deformed areas.

Figure 8 shows the crystallographic relationship between muscovite and potassium feldspar at a coherent interface. The SAED image shows how the crystallographic  $a$  axis of potas-

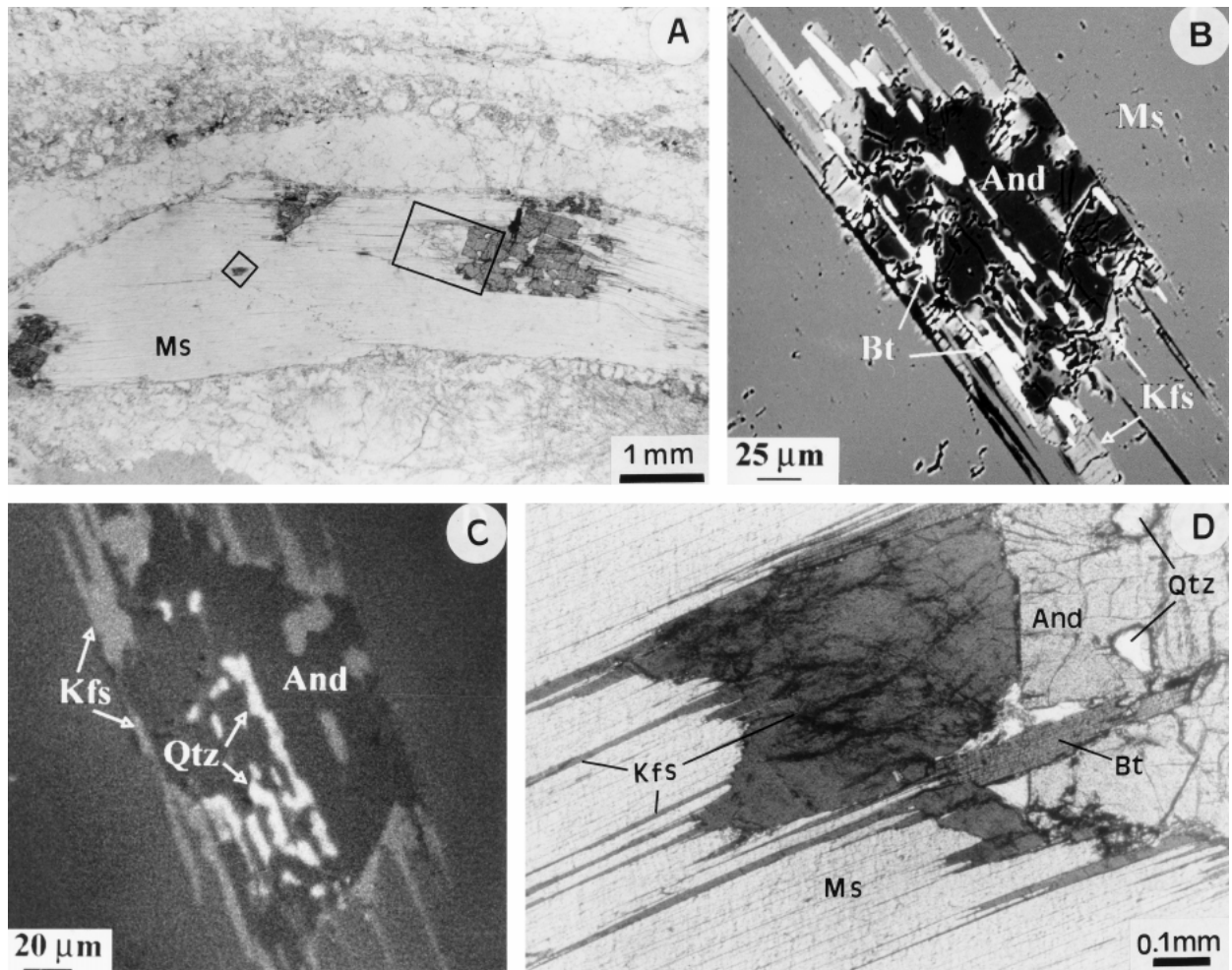


**FIGURE 2.** (A) Optical photomicrograph of a pegmatitic muscovite in banded gneisses, where diverse andalusite + potassium feldspar + quartz + biotite cores appear inside. (B) BSE image of an enlarged image of the incipient texture outline in A. Note the euhedral habit of the andalusite basal section and the location of potassium feldspar in the muscovite basal cleavages. (C) Si X-ray image showing the presence of quartz within the incipient texture. (D) A more evolved texture inside the same muscovite crystal where an andalusite single crystal appears surrounded by a potassium feldspar monocrystal that extends along the muscovite (001) basal cleavages (crossed polarizers).

sium feldspar coincides with one of the three equivalent directions  $\langle 110 \rangle / [010]$  of muscovite.

TEM analysis has revealed rutile intergrown with biotite, as well as iron oxides in open fractures between biotite and potassium feldspar. No crystallographic relationship has been observed between muscovite and biotite, with the exception of the coincidence of their  $c^*$  axes.

## DISCUSSION: MUSCOVITE DEHYDRATION REACTION

### Crystallography of the reaction

Structural control by muscovite on the nucleation and growth of its breakdown products has been described and discussed by authors such as Brearley (1986), Rubie and Brearley (1987), Worden et al. (1987), and Brearley and Rubie (1990). However, no detailed structural relationships have been presented between the muscovite host and the secondary minerals that

would allow the precise mechanism of the transformation to be established. Both epitaxy and topotaxy are feasible processes for explaining the observations of the above mentioned authors. The coincidence or parallelism between the planes of closest oxygen packing of the involved phases may be explained by epitaxy if the structural rearrangement is extensive (see for example Banfield and Eggleton 1988 for the transformation of biotite to kaolinite). In such a process, structural control by the muscovite substrate takes place on the growing phases at extensive defects such as shear planes or voids with surfaces parallel to the (001) planes of the muscovite crystals.

Structural relationships visible from the results of the optical and TEM study indicate that potassium feldspar and andalusite single crystals topotactically replaced pegmatitic muscovite crystals, at least in the early stages of the reaction process. Transformation took place with the least possible dis-

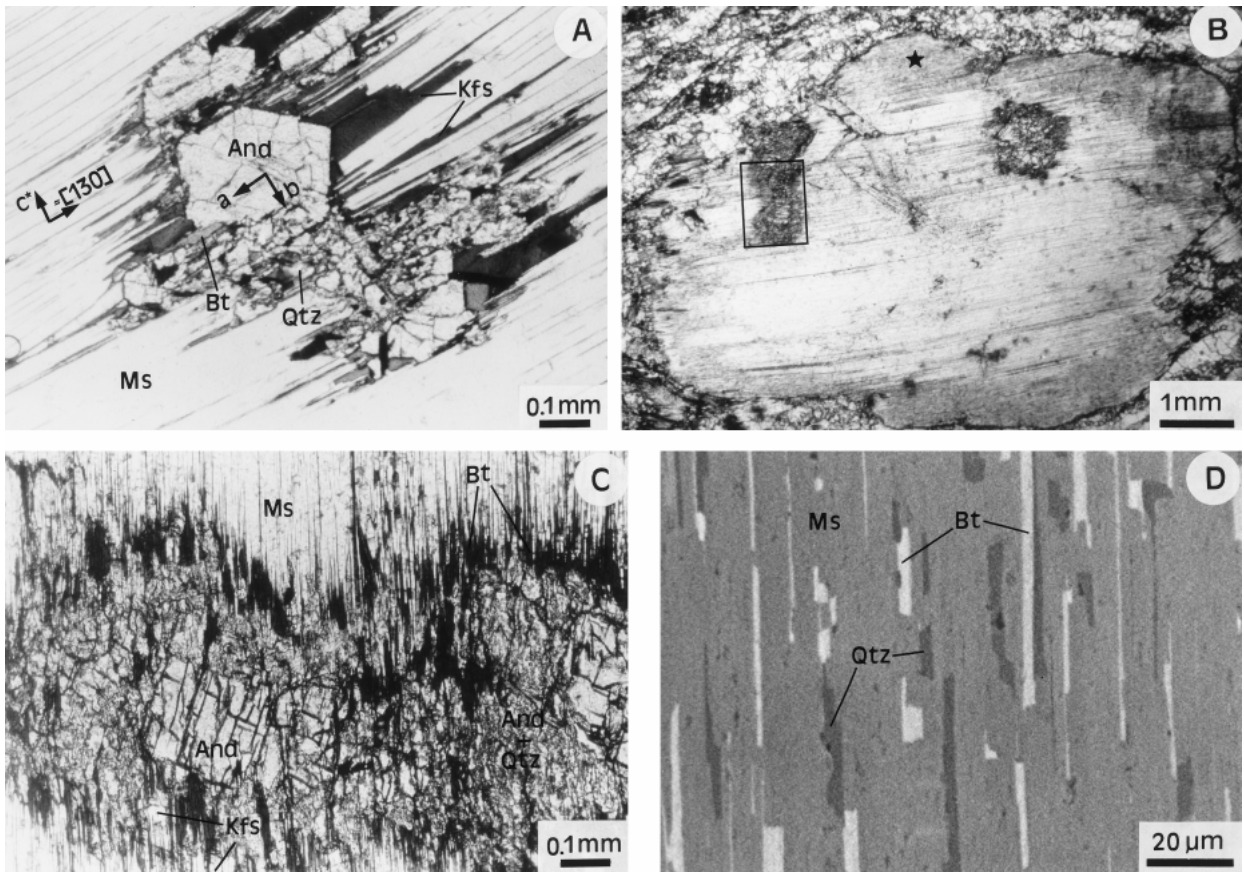


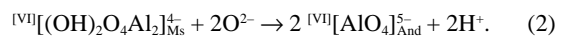
**FIGURE 3.** (A) Optical photomicrograph (crossed polarizers) of andalusite + potassium feldspar + quartz + biotite cores showing the euhedral habit of andalusite crystals and the coincidence of its *c* axis with [110] of the host pegmatitic muscovite. (B) Optical photomicrograph of a pegmatitic muscovite of the banded gneisses with muscovite breakdown textures within the crystal and decomposition reaction products in the rims. (C) Squared area in (B) showing an andalusite + potassium feldspar + quartz + biotite core that has reached the matrix, and where minor amounts of potassium feldspar occur in the muscovite cleavages. In addition, note how biotite crystals concentrate at the boundary between the core and the muscovite host. (D) BSE image of quartz + biotite intergrowths in the muscovite rims (star in B), produced after the phengitic decomposition reaction (Massonne and Schreyer 1987).

placement of ions and the least breaking of bonds. Structural fragments of the primary phase lattice have been used by the products of the breakdown reaction. Directions defined by strong bonds [periodic bond chains, PBC, of Hartman and Perdok (1955)] of the muscovite are preserved in potassium feldspar and andalusite. PBCs of the tetrahedral and octahedral sheets of the muscovite structure run respectively along the *a*\* (or <130>) and *b* (or equivalent <110>) axes. The coincidence of the *c* axis of andalusite with the <110> axis, or equivalent (Fig. 6), of muscovite implies that the andalusite lattice used PBCs from the octahedral sheet of the muscovite crystals. Crystallographic relationships between muscovite and potassium feldspar at coherent interfaces (Fig. 8) indicate that polyhedral chains from the tetrahedral sheet of muscovite are inherited by the potassium feldspar structure to form its crankshaft-like chains, as shown in Figure 9. Elemental reactions involved in the proposed structurally controlled reaction mechanism for the transformation of muscovite to andalusite and potassium feldspar are clearly not isochemical. In the simple

K<sub>2</sub>O-Al<sub>2</sub>O<sub>3</sub>-SiO<sub>2</sub> (KAS) subsystem, it is necessary to remove Al to form potassium feldspar from muscovite. In the same way Si and K must be removed to form andalusite from muscovite. Moreover, in the transformation of muscovite to potassium feldspar, not only must the destruction of the muscovite octahedral sheet, the migration of Al ions, and the redistribution of K ions in the potassium feldspar structure occur, but the remaining tetrahedral sheet must also be reorganized to provide the crankshafts of the new structure. This transformation yields two excess oxygen ions:



Similarly, there is no direct use of the muscovite octahedral layer by andalusite, as <sup>[VI]</sup>Al ions must be reordered in this sheet. Only two of the three PBCs along the *b* (or <110>) axis of the octahedral sheet may be used by the andalusite structure and there is a deficit of two oxygen ions in the transference of the octahedral PBCs:



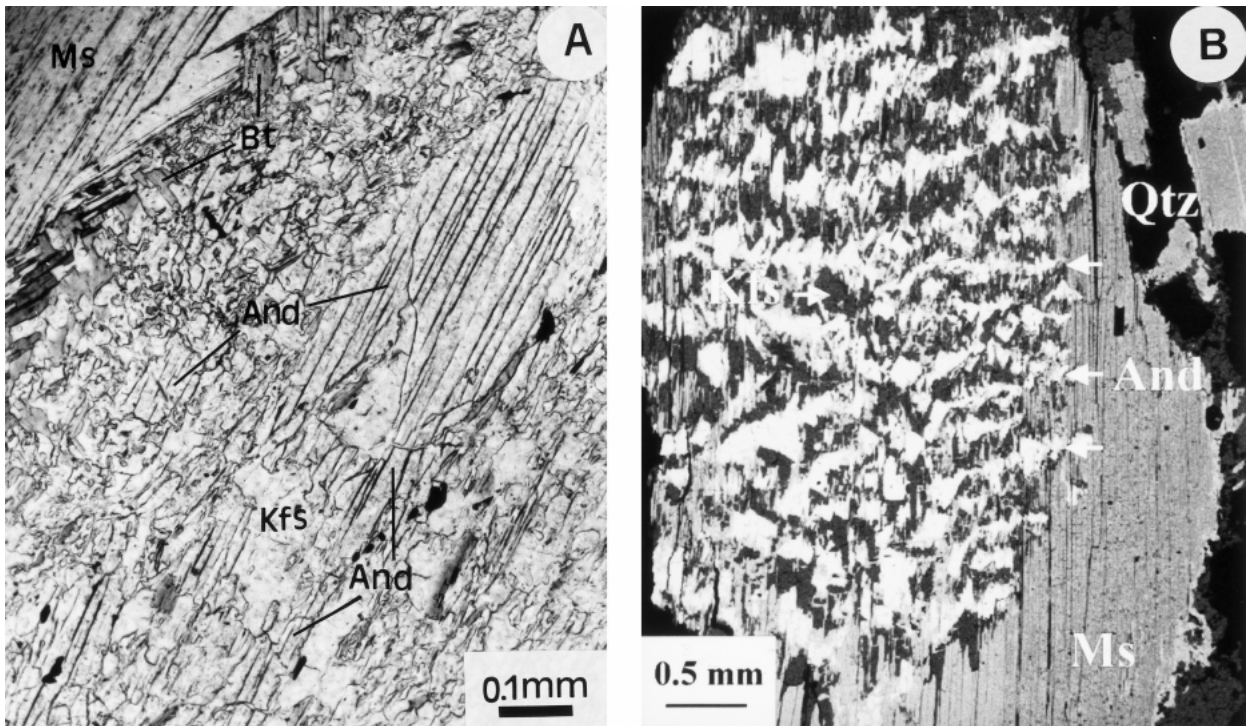


**FIGURE 4.** Breakdown textures in muscovites in pegmatitic bands from the TGC. (A) Optical photomicrograph of a muscovite crystal pseudomorphed by andalusite, preserving the basal cleavages, and occurring together with a group of disoriented muscovite crystals within a pressure shadow of a tourmaline porphyroblast having a diameter of 1.5 cm (not included in photograph). (B) Al X-ray image of alternating bands of andalusite (arrows) and potassium feldspar + biotite (dark bands) resulting from muscovite reaction with matrix quartz.

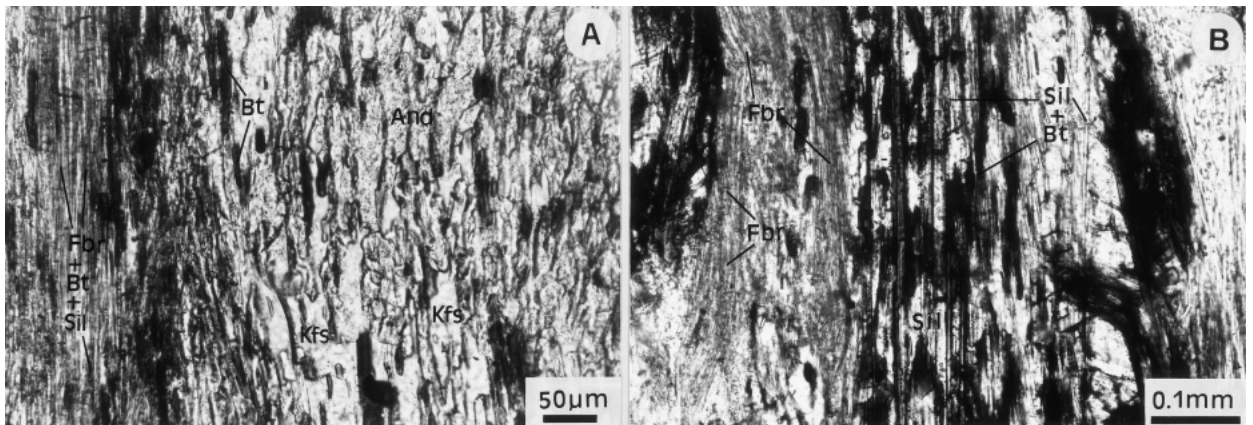


**FIGURE 5.** Optical photomicrograph of breakdown textures affecting old muscovite crystals located in quartzfeldspathic pods in pelitic gneisses from the Ronda peridotite aureole. (A) Old muscovite porphyroblast pseudomorphed by andalusite + potassium feldspar + biotite after breakdown. Elongated sillimanite prisms and fibrolite have grown from these biotite crystals at diverse areas of the texture where shear stress is preferentially located. (B) A similar, more evolved texture due to a major deformation; andalusite and potassium feldspar have disappeared completely.

As will be shown in the following section, a coupling between the two transformations might take place.

The lack of clear structural relations at the biotite-muscovite interface, with the exception of the coincidence of their  $c^*$  axes, the significant structural reorganization necessary for the

formation of biotite by direct modification of the muscovite structure, and the association of biotite with other precipitates, such as iron oxides, suggest an epitatic crystallization of biotite at planar defects parallel to the (001) muscovite planes. Structural continuity along octahedral sheets between the two

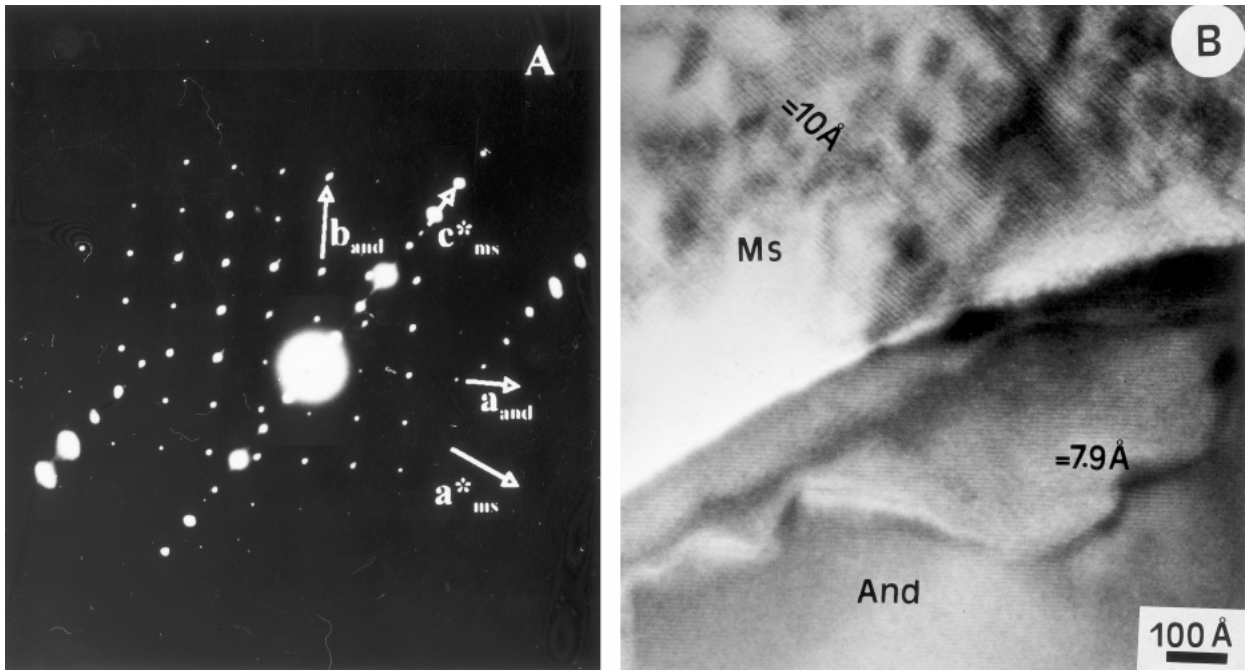


**FIGURE 6.** (A) SAED pattern at muscovite-andalusite interface showing approximate coincidence of andalusite *c* axis with  $\langle 110 \rangle$  (or  $\langle 010 \rangle$ ) of the muscovite ( $a_{ms}^*$  would correspond to  $[100]$  or equivalent  $\langle 130 \rangle$ ). (B) TEM micrograph of an incoherent interface between two phases of the area in which (A) was obtained. The slight disorientation between the two reciprocal planes is likely related to the development of grain boundaries after coarsening.

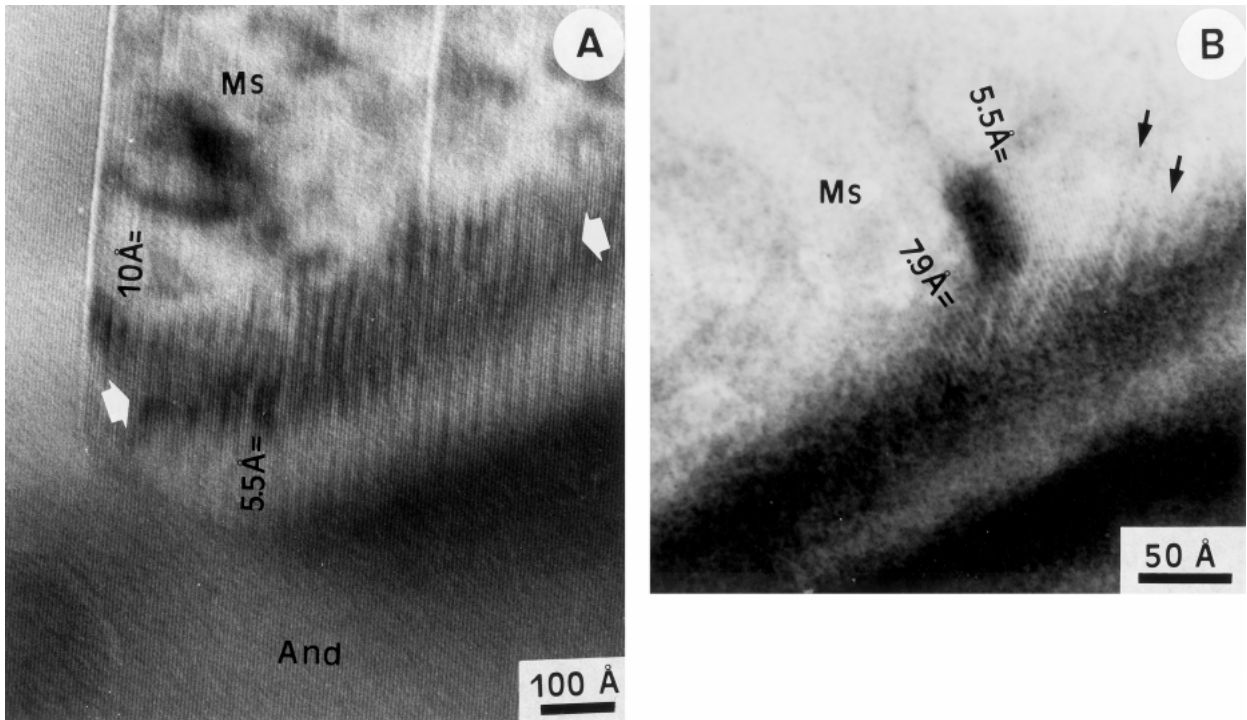


**FIGURE 7.** TEM images of coherent and semicoherent interfaces between andalusite and relict muscovite within it. (A) A coherent interface with a length of about 65 nm (arrowed) between the two phases where approximate parallelism between the (001) muscovite planes and the (110) andalusite planes may be observed. Strain energy at the interface is resolved through elastic bending of andalusite layers in interface vicinity. (B) Moiré fringe spacings around 1.5–2.2 nm (arrows) at a muscovite-andalusite semicoherent interface, where some crystallographic planes of the andalusite may be observed.

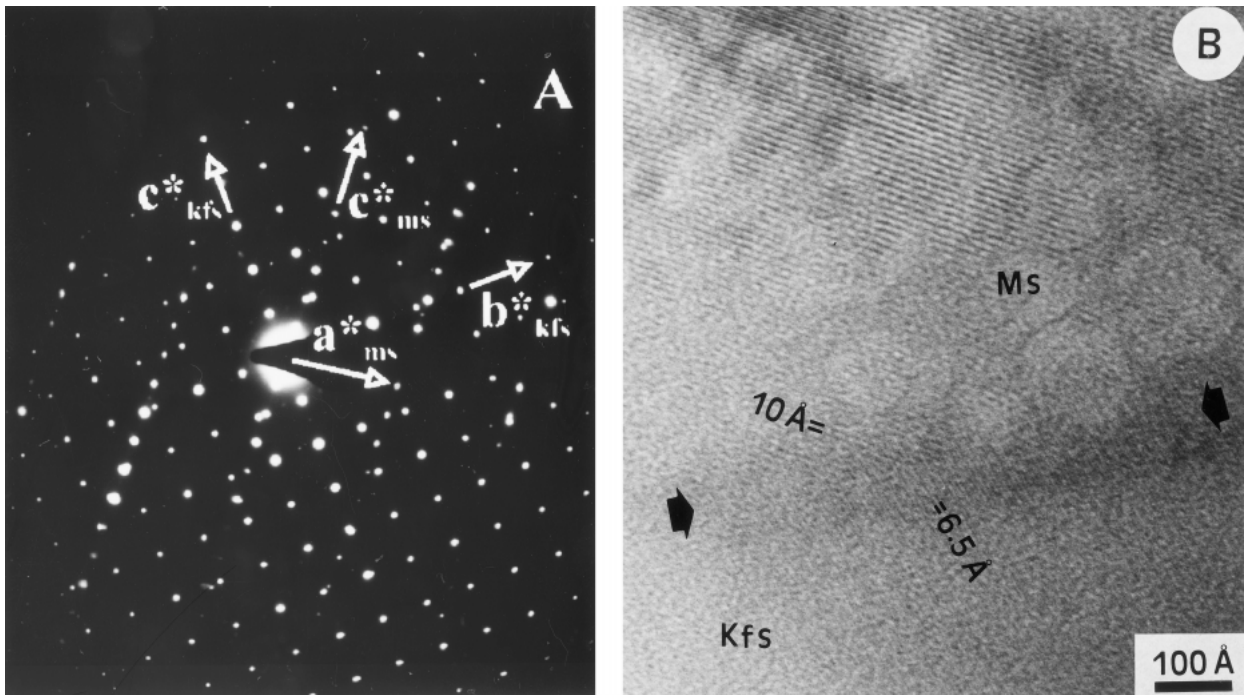


FIGURE 8. (A) SAED pattern at a muscovite-potassium feldspar coherent interface showing the coincidence of the potassium feldspar  $a$  axis with the  $b$  crystallographic direction (or equivalent) of muscovite (B) TEM image. Arrows indicate the interface.

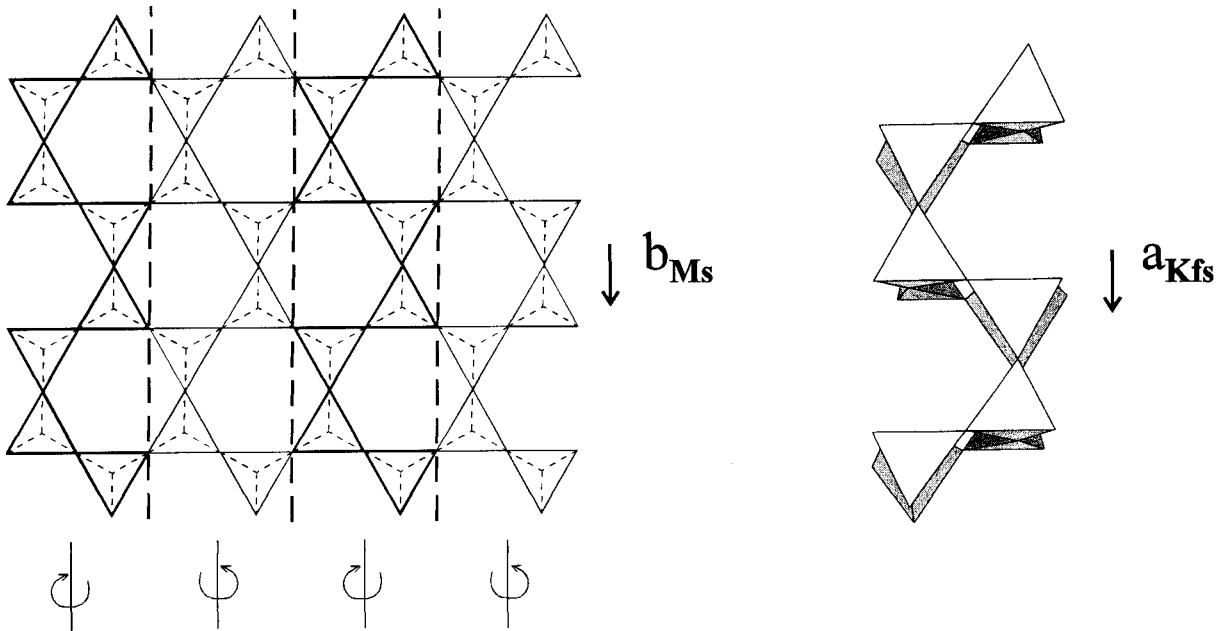


FIGURE 9. Possible mechanism for the formation of potassium feldspar crankshaft-like chains (righthand side of the figure) from muscovite tetrahedral sheet (lefthand side of the figure) through a three-step mechanism: (1) polyhedral chains of the muscovite tetrahedral sheet are individualized along  $b$ , after disruption of shared corners along the dashed lines; (2) rotation of tetrahedra of the individualized chains at the shared corners along the rotation axis indicated in the figure; and (3) corner sharing between tetrahedra from different sheets after destruction of the muscovite octahedral sheet and/or reorganization of the interlayer. The stoichiometry of this transformation considering only tetrahedra would be  $^{IV}[Si_3AlO_{10}]_{Ms} \rightarrow ^{IV}[Si_3AlO_{10}]_{Kfs}$ .

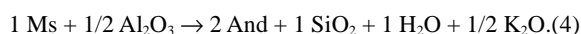
phases has been found by Iijima and Zhu (1982) in a specimen of intergrown crystals of muscovite and biotite, although no genetic relationship was established. Brearly (1986) also showed the crystallographic orientation relationship between biotite and potassium feldspar into muscovite pseudomorphs after breakdown reaction, with the coincidence of  $[010]_{\text{Bt}}$  and  $[100]_{\text{Kfs}}$ . In any event, this would not imply topotaxy if epitactic crystallization of biotite onto existing tetrahedral sheets of muscovite at a previous surface is considered.

### Reaction mechanisms and overall reaction

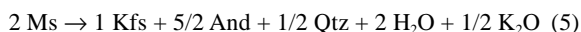
Elemental reactions (Lasaga 1981) for the direct transformations of muscovite to potassium feldspar and to andalusite conserving tetrahedral and octahedral cations respectively, as indicated in the above section for the initial structurally controlled step, may be written, in the KASH system, as:



and



For this possible mechanism andalusite forms not only from the topotactic replacement of muscovite as in reaction 4, but also from the reaction of 1/2 of the  $\text{Al}_2\text{O}_3$  remaining from Equation 3 with the adequate proportion of  $\text{SiO}_2$  from Equation 4. The excess  $\text{SiO}_2$  would precipitate as quartz. So, the reaction resulting from the sum of Equation 3 and Equation 4 would be:

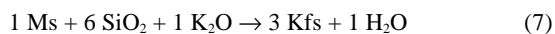


where the modal proportions of andalusite, potassium feldspar, and quartz correspond approximately with those observed in the incipient textures of Figures 2B, 2C, and 3A.

It is not possible to obtain reaction 5 through direct elemental reactions where all andalusite and potassium feldspar are formed from topotactic replacement of muscovite. Alternatively, all andalusite may be formed in this way if only 1/2 of the octahedral PBCs of muscovite are maintained, instead of 2/3 as in the case of elemental reaction 4, where all octahedral cations are conserved. The stoichiometry of such a transformation would be:



which is coupled with



where only 1/3 of the potassium feldspar is now formed from the topotactic replacement of muscovite.

This new mechanism, expressed by reactions 6 and 7, may also explain the precipitation of potassium feldspar in muscovite (001) basal cleavages. Therefore, due to the very slow diffusion of Si from the matrix through the muscovite lattice, the reaction proceeds by diffusion, in reverse direction, of  $\text{K}^+$  and  $\text{H}_3\text{O}^+$  ions through the interlayer, shear planes, or other surfaces parallel to the muscovite (001) planes. These surfaces may be considered as open spaces containing a  $\text{K}^+$ -rich aqueous fluid where potassium feldspar precipitation had occurred through reaction 7. The extent of this reaction would have been controlled by the relative flux of  $\text{K}^+$  to the matrix with respect to the total  $\text{K}^+$  liberated from reaction 6. So, reaction 5, explaining the observed modal proportion of andalusite, potas-

sium feldspar, and quartz, may be obtained via 5/6 (reaction 6) + 1/3 (reaction 7), which corresponds to a  $\text{K}^+$  flux equal to 2/5 of the  $\text{K}^+$  liberated in the direct transformation of muscovite to andalusite through reaction 6.

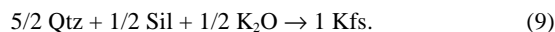
Reaction 5 is a particular solution of the equation system resulting from considering the Ms-Kfs-And-Qtz association in the KASH system, open for the  $\text{K}_2\text{O}$  and  $\text{H}_2\text{O}$  components. This equation system can be written vectorially as:



where x indicates number of moles.

The modal proportions  $n_{\text{Kfs}}$ ,  $n_{\text{And}}$ , and  $n_{\text{Qtz}}$ , measured on the observed textures, must satisfy the solution equation  $x_2 = 1/2(x_3 - x_4)$ . Solutions may involve the total absence of potassium feldspar or quartz as reaction products. The correspondence of the textural observations with the particular case represented by reaction 5 indicates that the direct elemental reactions, such as reactions 3 and 4 or reactions 6 and 7, which may have operated during the initial structurally controlled stage, continued after coarsening of the reaction products.

Potassium may react with the quartz and the unstable sillimanite in the matrix, after diffusion through the muscovite crystal, to produce potassium feldspar. So, for the K flux in reaction 5 we may write

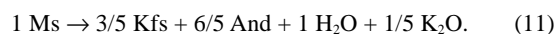


The overall reaction, resulting from the sum of reactions 5 and 9 will be

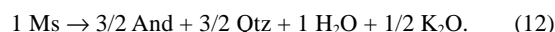


which implies the indirect transformation  $0.25 \text{ Sil} \rightarrow 0.25 \text{ And}$  for each mole of muscovite decomposed for the initial stages of the breakdown reaction. This indicates that the muscovite-out reaction would have been used to convert sillimanite to andalusite, due to the difficulty of the direct transformation of sillimanite to andalusite.

However, the increase in the modal proportion of quartz and the decrease in potassium feldspar with respect to andalusite observed in more evolved textures such as that in Figure 2D, as well as the drastic reduction of potassium feldspar when the reaction product of the muscovite core reaches the matrix (Figs. 1B, 1C, 3B, and 3C), indicate an important deviation from reaction 5. End-member reactions in the core of muscovite crystals correspond to the cases of minimum and maximum  $\text{K}^+$  flux. In the first case the maximum potassium feldspar production in the core takes place, which occurs when no quartz is produced in the core [i.e.,  $x_4 = 0$  in the solution equation  $x_2 = 1/2(x_3 - x_4)$  of reaction 8]. The reaction would be:



The other end-member reaction corresponds to the maximum K-flux and minimum potassium feldspar production in the core (i.e.,  $x_2 = 0 \leftrightarrow x_3 = x_4$  in Eq. 8). This solution is expressed by the reaction:

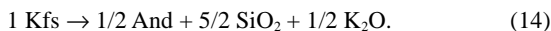


The K-fluxes originating in the muscovite core through reactions 11 and 12 would produce, after reaction with the matrix sillimanite and quartz, the transformation of 0.2 and 0.5 moles, respectively, of sillimanite to andalusite for each mole

of muscovite decomposed through the reaction:

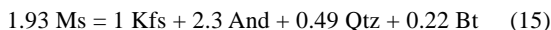


Because reaction 5, observed for the incipient textures, is an intermediate case between reactions 11 and 12, and it is possible to pass from reaction 11 to 12 by potassium feldspar dissolution to produce andalusite, quartz, and  $\text{K}_2\text{O}$  through the reaction:



It may be envisaged that, for the more evolved textures that reached the matrix, a sequential mechanism occurs in which first an assemblage with only potassium feldspar and andalusite is produced in the muscovite core, and then a pressure-solution process transforms a certain proportion of potassium feldspar into andalusite plus quartz.

Consideration of the intergrowth biotite within the muscovite cores together with the rest of the phases allows us to envisage the reaction mechanism in terms of a nearly constant-volume process. Therefore, in the case of the lowest-evolved texture shown in Figures 2A–C, the modal analysis performed on BSE and X-ray images gives 2170, 1971, 202, and 600 pixels for andalusite, potassium feldspar, quartz, and biotite, respectively. Using molar volumes for the phases involved at 2 kbar and 600 °C, we can obtain, when normalized to one mole of potassium feldspar, the following constant-volume reaction:



which compares well with the above Al-conservative reaction 5 in the KASH system. Biotite would have formed from the  $\text{MgO}$ -,  $\text{FeO}$ -, and  $\text{TiO}_2$ -components in muscovite, from part of the  $\text{Al}_2\text{O}_3$  and  $\text{SiO}_2$  employed in the formation of andalusite and quartz, and from part of the  $\text{K}_2\text{O}$  and  $\text{H}_2\text{O}$  liberated in the reaction process. In any event, the process may also be considered quasi-constant-volume.

### Kinetics of reaction

**Diffusion-control vs. surface reaction-control.** In the previous section the reaction in the muscovite core was shown to be balanced by K diffusion through the muscovite crystal to the matrix. The diffusion of K outward from the biotite crystals and the immobility of Si, Al, Fe, Mg, and Ti has been demonstrated by Eggleton and Banfield (1985) for the solid-state transformation of biotite to chlorite through a topotactic replacement (mechanism 2 in Veblen and Ferry 1983). The Si-, Al-, Fe-, Mg-, and Ti-conservative character of the muscovite breakdown reaction is based on the very slow diffusion of these elements through the muscovite lattice. This is due to the high site energy of the tetrahedral and octahedral cations and the low anion porosity of these sheets (Dowty 1980; Smyth and Bish 1988). However, lattice diffusion of the interlayer cations, especially parallel to the mica layers, is clearly favored by these crystal-chemical factors affecting ion mobility in the crystal structure of the mica. The marked anisotropy of diffusion through the mica lattice has been demonstrated by Fortier and Giletti (1991), whose results indicate that the oxygen self-diffusion coefficient perpendicular to the layers is three to four orders of magnitude lower than for transport parallel to the mica layers.

As indicated above, the existence of planar defects creates high-diffusivity paths parallel to the mica layers. These defects can cause strong deviations from ideal stoichiometry, with the production of vacancies and interstitials that aid lattice diffusion. Chemical defects, called crystallographic shear planes (Veblen 1992), may occur in the mica structure parallel to (001) in the interlayer level, with the collapse or dilation of the structure across the planar boundary (Amouric 1987; Sánchez-Navas and Galindo-Zaldívar 1993). The substitution of  $\text{K}^+$  ions by  $\text{H}_3\text{O}^+$  at the interlayer level allows the formation of a film of fluid at such planar defects. A duolayer of adsorbed molecules ( $\sim 10$  Å), as suggested by Walther and Wood (1984), may form this film. Therefore, instead of lattice diffusion we can consider diffusion through a fluid film, controlled by the solubility and diffusivity of the solute in the fluid. Since basal slips commonly occur between the different packets or coherent domains of the phyllosilicate structure (Nieto and Sánchez-Navas 1994), without disruption of the crystal structure (Sánchez-Navas and Galindo-Zaldívar 1993), only a certain proportion of the slips produce fractures or open areas subparallel to the packet boundaries, where a fluid film may be located.

To evaluate the diffusion of K through this fluid film, we need to know the porosity for grain boundary diffusion,  $\phi$ , defined as the fractional volume occupied by a fluid, and expressed as the product of the length of the grain boundary per  $\text{cm}^2$  ( $l$ ) by the width of the fluid film ( $d$ ). In this work, the intracrystalline porosity along the directions perpendicular to the mica  $c^*$  axis has been established from the morphology and the estimation of the proportion of microcleavages deduced from TEM observations. To determine the proportion of these kinds of defects, we can first consider the frequency of planar defects in general along the mica  $c^*$  axis. A planar defect commonly observed in the TEM images of phyllosilicates is twinning on the composition plane (001). This produces a change in the packet contrast on TEM images, due to the change in the orientation of crystallographic directions  $a$  and  $b$  in the basal plane between the packets or coherent domains of the crystal. Similar effects are produced by deformational defects such as basal slips at the interlayer level. These coherent domains have a thickness near 1  $\mu\text{m}$  along  $c^*$  in these pegmatitic crystals.

However, only lenticular voids resulting from basal slip in the interlayer level are considered to be planar defects that allow diffusion through a fluid film, and they may account for less than a tenth of the total planar defects observed along the  $c^*$  axis. These voids average 10 Å in thickness across the mica layers and 1000 Å in length [see Fig. 8 in Amouric (1987), and Fig. 7 in Sánchez-Navas and Galindo-Zaldívar (1993) for the case of deformed biotite crystals; and Fig. 7 in García Casco et al. (1993) for the deformed matrix muscovites of these rocks]. The finite character of such voids parallel to the layers, when compared with other planar defects in mica, reduces the probability of finding this defect along these directions by at least one tenth. All this leads to considering a length of microcleavage boundaries,  $l$ , equal to

$$\frac{0.1 \mu\text{m}}{1 \mu\text{m}^2} \frac{1}{10} = 10^{-3}/\mu\text{m} = 10/\text{cm}$$

which gives an intracrystalline porosity,  $\phi$ , of  $10^{-6}$  ( $10/\text{cm} \cdot 10^{-7}$

cm) for the muscovite planes parallel to  $c^*$ . Substitution of this  $\phi$  value in the equation:

$$L_{KK}^D = \frac{D_{KK} C_K}{RT} \phi \quad (16)$$

of Walther and Wood (1984), where  $L_{KK}^D$ ,  $D_{KK}$ , and  $C_K$  are the phenomenological coefficient, diffusion coefficient and concentration, respectively, for the case of the  $k$  components, and using a  $D$  equal to  $10^{-4}$  cm<sup>2</sup>/s (Brady 1983; Lasaga 1986) and a concentration of  $10^{-4}$  mol/cm<sup>3</sup>, corresponding to the solubility of quartz at 600 °C and 2 kbar (Fournier and Potter 1982), gives, after changing units:

$$\left( L_{KK}^D = \frac{10^{-8} \text{ m}^2/\text{s} \cdot 10^2 \text{ mol}/\text{m}^3}{8.3144 \text{ J} / \text{K mol} \cdot 873 \text{ K}} 10^3/\text{m} \cdot 10^{-9} \text{ m} \right) \\ = 1.38 \cdot 10^{-16} \text{ mol}^2/\text{J} \cdot \text{m} \cdot \text{s}$$

This value is much greater than that obtained when considering diffusion through defective areas formed by the disorganization of layers between the mica packets (see Walther and Wood 1984, for the value of their true grain boundary diffusion coefficient) or a lattice diffusion process.

If the overall rate of mineral growth in the muscovite core is controlled by the diffusion rate of the K interlayer cations (see later discussion), it is necessary to know, besides the magnitude of the diffusion coefficient (which depends, as seen, on the type of transport considered through the mica), the chemical potential gradients between the core and the matrix assemblages that drives the diffusion process (Fisher 1973 and 1977). The matrix and core assemblages are related through reactions 9 and 5 respectively, from which the relationship

$$\Delta\mu_K^{5-9} = \mu_K^5 - \mu_K^9 = \Delta G_{\text{Muscovite out}} + 1/4 \Delta G_{\text{Sill-And}}$$

may be obtained. Therefore, the driving force for the K flux may result not only from the overstepping of the muscovite-out reaction but also from the difference in free energies of andalusite and sillimanite under  $P$ - $T$  conditions where andalusite is stable. Fisher (1970) studied mineral segregations originated from chemical potential gradients that resulted simply from the difference in free energy between these polymorphs, with andalusite being the stable phase.

Determination of the exact values of  $P$  and  $T$ , and so of both  $\Delta G_r$ , from the relative rates of reaction 13 and the polymorphic transformation, is not possible due to lack of data on the kinetics of the Sill  $\rightarrow$  And reaction. Despite experimental studies on the andalusite-sillimanite reaction kinetics, such as the work of Nitkiewicz (1989), the rate law for this transformation has not been established due to its sluggishness. In fact, this reaction is significantly slower and has a smaller  $\Delta G_r$  than the other two polymorphic reactions (Kerrick 1990). On the other hand, a precise rate law has been established experimentally for the dehydration of muscovite + quartz (Schramke et al. 1986; Lasaga 1986). In accordance with Lasaga (1986) and the considerations of Kerrick et al. (1991) regarding the existence of a non-linear relationship between the reaction rate and the  $\Delta G_r$ ,

of the type of the Arrhenius-based equation for the andalusite-sillimanite reaction, it is possible to apply a “general” surface rate law for the andalusite growth rate of type  $k \cdot \Delta G^2$ . Application of this law to the present case means that the  $P$ - $T$  conditions examined would produce overstepping of the two considered reactions such that  $\Delta G_{\text{Muscovite out}} \approx 2 \Delta G_{\text{Sill-And}}$ , if the same pre-exponential factor  $k$  is considered for both cases. Determination of  $\Delta\mu_K^{5-9}$  has been done, after calculation of  $\Delta G_r$  using the VERTEX program of Connolly and Kerrick (1987) and the thermodynamic data base of Holland and Powell (1990), for the cases of 3 kbar and 639 °C ( $\Delta G_{\text{Muscovite out}} \approx 2.5 \Delta G_{\text{Sill-And}}$ ) and 2 kbar and 605 °C ( $\Delta G_{\text{Muscovite out}} \approx \Delta G_{\text{Sill-And}}$ ), where the muscovite-out reaction has been overstepped by 5 °C in both cases, which gives  $\Delta\mu_K^{5-9}$  values of 389.2 and 482.2 J/mol, respectively.

The rate law, relating core size with time, for the muscovite breakdown process controlled by the intracrystalline diffusion of  $K^+$  ions has been derived in the Appendix, following Fisher (1978). The equation obtained, expressing the time  $t$  (in seconds) as a function of the core size,  $X_C$ , is

$$t = \left( \frac{3}{8} L \frac{v_K^{(5)}}{v_{Ms}^{(5)}} \frac{1}{L_{KK}^D \Delta\mu_K^{5-9} v_{Ms}} \right) X_C - \left( \frac{3}{16} \frac{v_K^{(5)}}{v_{Ms}^{(5)}} \frac{1}{L_{KK}^D \Delta\mu_K^{5-9} v_{Ms}} \right) X_C^2 \quad (17)$$

where parameters  $L$ ,  $v_K^{(5)}$ ,  $v_{Ms}^{(5)}$ , and  $v_{Ms}$  are the length of the muscovite crystal measured along the basal layers, the stoichiometric coefficients of K and Ms in reaction 5 and the molar volume of muscovite, respectively. Equation 17, corresponding to a parabola, has physical significance only in the interval  $[0, L]$ . The fact that the core grew at the expense of the host muscovite crystal, increasing the reaction and diffusion surfaces, means that the greatest growth rates corresponded to the final stages. Making  $L$ ,  $v_K^{(5)}/v_{Ms}^{(5)}$ , and  $v_{Ms}$  equal to 0.01 m, 1/2 and  $1.428 \cdot 10^{-4}$  m<sup>3</sup>/mol, and using the values of  $1.38 \cdot 10^{-16}$  and  $1.33 \cdot 10^{-16}$  mol<sup>2</sup>/J·m·s for  $L_{KK}^D$  and of 482.2 and 389.2 J/mol for  $\Delta\mu_K^{5-9}$  corresponding to the two previously considered  $P$  conditions of 2 and 3 kbar respectively, Equation 17 yields a time between 11 300 and 14 500 years for the core diameter of 0.002 m observed in the most evolved textures that have not yet reached the matrix (Figs. 2A and 2D). The time of about 10 000 years seems to be a reasonable time constant for thermal decay in a pluton contact aureole (Spear 1993).

As indicated in the introduction section, Lasaga (1986) has demonstrated that the muscovite dehydration reaction is surface-controlled both in laboratory experiments and in field situations. The low solubility of aluminosilicates causes the dissolution rate at the mineral surface of andalusite and not the diffusion transfer, to control the overall rate. Applying the reaction data of Lasaga (1986) to model the reaction textures presented here (see Appendix) provides the following linear growth law:

$$t = 4.03 \cdot 10^{12} r \text{ (sec)} \quad (18)$$

This law yields a time of 12 800 years for a basal thickness of 2 mm ( $r = 0.1$  cm in andalusite crystals), such as that observed in the most evolved textures (Figs. 2A and 2D). This result is very similar to that obtained with the above rate law deduced for a diffusion-controlled process. Figure 10 shows the diffusion-reaction boundary, indicating the transition from reaction-

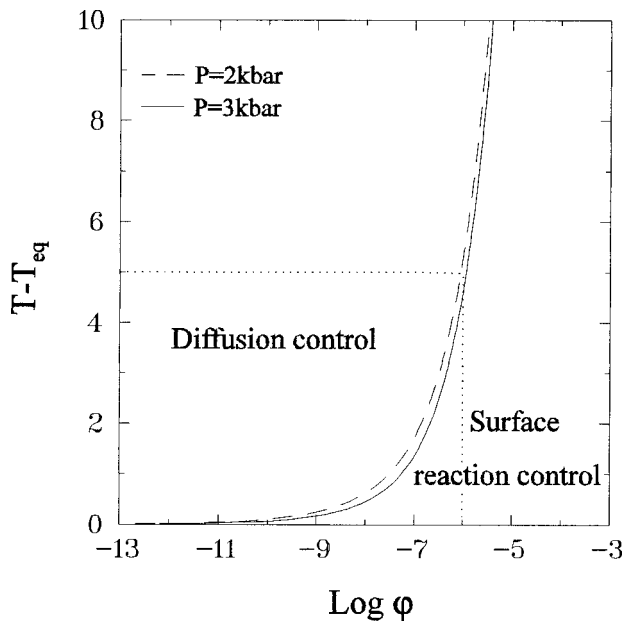


FIGURE 10. Temperature overstep required for diffusion to match reaction rates as a function of intracrystalline porosity,  $\phi$ . The temperature overstep of 5 °C and  $\phi$  equal to  $10^{-6}$  considered for this natural case plot just on the diffusion-surface reaction boundary.

controlled to diffusion-controlled processes, as a function of temperature overstep and intracrystalline porosity ( $\phi$ ) for the equilibrium conditions at 2 and 3 kbars, in a manner similar to that in Figure 6 of Lasaga (1986). For this the two previously deduced rate laws for diffusion-control and reaction-control models have been equated after expressing time as a function of temperature overstep and diffusion coefficient  $L_{KK}^D$  (or intracrystalline porosity) as shown in the Appendix. As presented in Figure 10, the conditions of temperature overstep and porosity considered here in this natural case plot just on the diffusion-surface reaction boundary. However, the overall rate seems to be controlled by diffusion transfer as indicated by the considerations given below. Therefore, although dehydration reactions require very low overstepping for nucleation (Ridley and Thompson 1986) and growth (Lasaga 1986), particularly when topotactic replacement of the reactants by products occurs, the value of the temperature overstep assumed here (5 °C) is probably extremely low. In fact, Ridley and Thompson (1986) suggest that nucleation generally takes place after 10–50 °C of overstepping for a dehydration reaction. In laboratory experiments on the muscovite breakdown reaction, Rubie and Brearley (1987) and Brearley and Rubie (1990) also observed crystallographic relationships between the phases under conditions of marked overstepping of temperatures. The porosity considered for this natural case in Figure 10 may be low for an intracrystalline diffusion process and it represents a maximum value for the diffusion coefficient. The size and the idiomorphic morphologies of the andalusite single crystals in the cores would result from a slow removal rate of the components that could not be accommodated in the core ( $K_2O$  and  $H_2O$  in this case). In addition, the relatively quick non-reconstructive struc-

tural replacement favored the dissolution and growth of the aluminosilicate phases in spite of their low solubilities.

The macroscopic development of these textures (e.g., Fig. 1A) indicates that core growth by diffusion continued for a significant time interval, as seen in the preceding section, indicating that the assumption that reaction 9 in the matrix proceeded at such a rate that all the K supplied by the muscovite core reaction 5 was consumed is correct. This supports the idea that the process may approach a state of minimum entropy production, equivalent to a steady state (Fisher 1973).

**Sequential kinetics and other kinetic considerations.** Structural relationships discussed in a preceding section indicate that a certain degree of lattice matching across the muscovite-potassium feldspar and muscovite-andalusite interfaces might exist in the incipient stages of the reaction. The similarity of their structural elements allows an initial coherence, which means that the activation energy for nucleation is small. TEM study has shown the preservation, in spite of coarsening, of some coherent relict interfaces between muscovite and potassium feldspar (Fig. 8B) and between muscovite and andalusite (Fig. 7A), which probably formed part of a major stepped interface formed in the early stages of the reaction process. However, coarsening increased the strain energy due to the structural differences between the muscovite host and the reaction products, although this effect may have been reduced by the appearance of dislocations at the interface. The relaxation of the coherence strain when the critical thickness is reached ( $\sim 700$  Å for the muscovite-andalusite interfaces, as seen in Fig. 7A) favors the formation of semicoherent interfaces. In these cases Moiré fringes appear, such as occurs in the muscovite-andalusite interface in Figure 7B. These fringes are due to a more or less regular spacing of the misfit dislocations, which produce local plane bending (Dixon et al. 1992). The difficulty for a coherent or semicoherent planar interface to migrate, due to the unstable, high-energy situation produced by the simple incorporation of a new atom (Putnis 1992), indicates the existence of an initial interface-controlled growth of reaction products in the muscovite crystal core. However, it must be taken into account that the partial non-reconstructive character of the transformations described in this paper notably reduce the thermal activation barrier for the interface motion. The formation of non-coherent interfaces, after coarsening of the reaction products, causes the growth process to be controlled by diffusion of the K component removed from the core through the muscovite crystal.

As shown in the section on the muscovite breakdown textures, some muscovite single crystals in pegmatitic rocks from the TGC, where sillimanite is absent, are replaced by andalusite and potassium feldspar forming alternating bands (Fig. 4B). These textures may be explained by a diffusion-controlled Liesegang-type mechanism where diffusion of chemical species is coupled with an internal precipitation process (Fisher and Lasaga 1981). Interaction between the diffusive fluxes, possibly of K and Si, across an initial muscovite-quartz boundary perpendicular to the muscovite basal layer, would produce the supersaturation products necessary for the precipitation of the phases and the formation of observed bands.

Textural analysis also shows that the reaction took place

only when overstepping was locally enhanced by the underpressure produced at pressure-shadow areas by differential stress. This is particularly high at competent layers (Robin 1979) and in relation to porphyroblasts (Strömberg 1973). So, the minimum principal stress,  $\sigma_3$ , would have a low value in the quartzo-feldspathic pegmatitic layers, and in the pressure shadows associated with pegmatitic muscovite crystals occurring within a shear zone. Deformation affecting pegmatitic muscovite crystals also produced open spaces such as voids in the hinge zones and serrated boundaries of minor folds with kink geometry (not shown here), which acted as points for heterogeneous nucleation of the reaction products. This would explain why the dehydration reaction does not affect muscovite crystals in the matrix in spite of the low magnitude of overstepping necessary to promote this type of reaction. The pressure solution produced the segregation of potassium feldspar at the pressure shadows of the muscovite crystals in deformed banded gneisses.

The local increase of the free-energy change of the reaction due to underpressure, the reduction of the activation barrier due both to the low interfacial free energy of the coherent interfaces and to the non-reconstructive character of the reaction, the large entropy and volume change of the reaction, and the high absolute temperature at which it took place, all indicate that overstepping of the muscovite dehydration reaction boundary might be small. The existence of initial interface-controlled growth followed by diffusion-controlled growth is in accordance with a low overstepping reaction before nucleation, as shown by Ridley and Thompson (1986).

The occurrence of less-evolved textures together with more-evolved ones is due to the fact that nucleation was not instantaneous but continued in an apparently random fashion almost to reaction completion, and also due to the buffering process. The reaction was stopped by the reduction in temperature as energy was absorbed by this endothermic reaction (Ridley 1985) and by the local overpressures produced by fluid liberation (Dutrow and Norton 1995). Therefore, local fluctuations in fluid pressure through a process of opening and filling of microcracks by reaction products (Etheridge et al. 1984) may produce pulsating episodes of nucleation and growth even inside muscovite crystals.

It may be deduced from the above discussion that although heat flow may have been significant when the well-developed diffusion-controlled structures formed, low thermal inertia may be supposed for the heat source. In this respect, rapid heat transport by fluids through an important regional shear zone connecting these rocks with adjacent granitic rocks, generated during peridotite emplacement, may be considered as the driving force for this reaction, as will be examined in more detail in the next section. It explains the fact that the pegmatitic crystals localized at highly deformed mylonitic bands of the TGC have been affected selectively by the dehydration reaction.

#### **PETROLOGICAL CONSIDERATIONS AND CONCLUDING REMARKS**

The slight overstepping of the muscovite-out reaction deduced for the gneissic rocks of the TGC contrasts with the observations on equivalent textures in pelitic gneisses from the

Ronda peridotite aureole, where all muscovite has been completely pseudomorphed by andalusite, potassium feldspar, and biotite. These rocks, belonging to two structurally equivalent nappes and therefore affected by the same geotectonic processes, share a decompression path that crosses the three polymorph fields, from kyanite to andalusite through the sillimanite field (Torres-Roldán 1981; García-Casco et al. 1993). This decompression path is recorded by the compositional trends shown for the matrix muscovite in banded gneisses from the TGC (García-Casco et al. 1993). Pegmatitic muscovite crystals must constitute, together with other minerals such as porphyroblasts of potassium feldspar and some biotites from the orthogneiss, original mineral phases of an old Hercynian granite (Sánchez-Navas, in preparation). Due to the large size of the pegmatitic muscovite crystals, they must have acquired the chemical signature of the medium-pressure Alpine event only at their rims, where the celadonic decomposition reaction is observed, whereas smaller matrix muscovite crystals equilibrated easily at these metamorphic conditions. Products of this reaction are biotite, quartz, and rutile (and at low pressures ilmenite), whereas potassium feldspar nucleated at the matrix after K diffusion to the matrix. The fact that the breakdown reaction occurred at low-pressure conditions in the andalusite stability field resulted in decomposition of non-celadonic cores of muscovite crystals, whereas celadonic-rich matrix muscovite crystals were unaffected. This is in agreement with the fact that the celadonic component of muscovite produces a displacement of the breakdown equilibrium toward higher temperatures for a given pressure (see Fig. 5D of Anderson and Rowley 1981).

The decompression process was accompanied by the development of a significant penetrative foliation (Torres-Roldán 1981; Tubía and Cuevas 1986; Cuevas et al. 1989) where fibrolitic sillimanite grew and formed a lineation defined in some cases by prismatic sillimanite in highly deformed shear zones, over which andalusite grew at low pressure through a coalescence mechanism (Sánchez-Navas unpublished data). This, together with the observation of sillimanite prisms and fibrolite growing from biotite in completely transformed muscovite pseudomorphs (Figs. 5A and 5B), indicates that the pelitic gneisses from the Ronda aureole were affected, after the decompression process, by a heating event at low-pressure conditions where the muscovite-out and  $\text{And} \rightarrow \text{Sill}$  reactions were crossed sequentially. Less heating would have taken place for the gneisses from the TGC. In this case the sillimanite field was not reached after muscovite breakdown, and fibrolite probably grew before muscovite breakdown, either within its stability field during a decompression process accompanied by deformation (as indicated above), or metastably at low pressure within the andalusite stability field (Kerrick 1987), stabilizing and concentrating in the folia under high non-coaxial strains (Wintsch and Andrews 1988) associated with the late crustal emplacement of peridotites (see below).

Metastable fibrolitic sillimanite would have developed during the heating responsible for the muscovite breakdown reaction, which was produced by the low-pressure contact metamorphic episode related to the high-temperature emplacement of the Ronda peridotite (Loomis 1972a, 1972b; Lundeen 1978; Tubía and Cuevas 1986). This fibrolite was formed and

concentrated in folia, through a base-cation leaching process (Vernon et al. 1987; Vernon 1987b; Kerrick 1990) during an influx of hot, acidic fluids generated during the emplacement of intrusive leucogranites from the underlying Blanca unit (Currás and Torres-Ruiz 1992; Acosta and Menéndez 1995; Shaw et al. 1996). A fluid-migration mechanism through a regional shear zone (such as that envisaged by Etheridge et al. 1983), associated with the emplacement of the ultramafic sheet through a compressional tectonic injection mechanism (Sánchez-Navas and Martín-Algarra unpublished data), produced a rapid heating-cooling event in the studied rocks, which explains the observed textures and the occurrence of the large andalusite zones of adjacent metamorphic terrains. All this is in agreement with the idea of Rubie (1986) that the development of equilibrium (or near-equilibrium) mineral assemblages and microstructures generally occurs over relatively short periods of time under transient fluid-present conditions.

It may be concluded that, although this reaction took place at low degrees of overstepping for the gneissic rocks of the TGC, in part due to buffering processes such as the endothermic character and fluid pressure oscillations associated with the chemical reaction itself, significant overstepping of the reaction boundary is deduced from the muscovite-out textures in pelitic gneisses from the Ronda aureole. In this case andalusite together with biotite and potassium feldspar topotactically replaced muscovite crystals that have been completely transformed. Growth of elongated and disoriented sillimanite crystals on biotites of the matrix and of muscovite pseudomorphs, and on matrix andalusite are also observed. This points to a possible rapid heating and cooling of these rocks after decompression. This regional contact metamorphism was produced by the late-crustal emplacement of peridotites, perhaps through a compressional tectonic injection mechanism of the ultramafic sheet, at an approximate depth of 7–10 km during the exhumation process of these rocks, followed by late-orogenic extension.

### ACKNOWLEDGMENTS

I thank Antonio C. Lasaga for his suggestions on the first version of the manuscript, and R.J. Tracy, C.T. Foster, and R.M. Dymek for their critical and constructive comments, which have improved this paper. I also want to acknowledge the help received from M.M. Abad and M.A. Hidalgo of the C.I.C. at Granada University, from my colleagues in the Department and especially from F. Nieto. I am also thankful to A. Martín-Algarra. I am indebted to Christine Laurin for revising the English text. This work was financed by Research Project PB96-1383 (CICYT, Spain) and is a contribution of Research Group RNM 268 of the Junta de Andalucía.

### REFERENCES CITED

- Acosta, A. and Menéndez, L.G. (1995) Melting and Generation of Leucogranite Associated with the Emplacement of Ronda Peridotites. In M. Brown and P.M. Piccoli, Eds., The origin of granites and related rocks. U.S. Geological Survey Circular, 1129, 7–8.
- Amouric, M. (1987) Growth and deformation defects in phyllosilicates as seen by HRTEM. *Acta Crystallographica*, B43, 57–63.
- Anderson, J.L. and Rowley, M.C. (1981) Synkinematic intrusion of peraluminous and associated metaluminous granitic magmas, Whipple Mountains, California. *Canadian Mineralogist*, 19, 83–101.
- Banfield, J.F. and Eggleton, R.A. (1988) Transmission electron microscope study of biotite weathering. *Clays and Clay Minerals*, 36, 47–60.
- Brady, J.B. (1983) Intergranular diffusion in metamorphic rocks. *American Journal of Science*, 283A, 181–200.
- Brearely, A.J. (1986) An electron optical study of muscovite breakdown in pelitic xenoliths during pyrometamorphism. *Mineralogical Magazine*, 50, 385–397.
- Brearely, A.J. and Rubie, D.C. (1990) Effects of H<sub>2</sub>O on the disequilibrium breakdown of muscovite + quartz. *Journal of Petrology*, 31, 925–956.
- Connolly, J.A.D. and Kerrick, D.M. (1987) An algorithm and a computer program for calculating composition phase diagrams. *CALPHAD* 11, 1–54.
- Cuevas, J., Navarro-Vilá, F., and Tubía, J.M. (1989) Interprétation des cisaillements ductiles vers le NE dans les gneiss de Torrox (Complexe Alpujarride, Cordillères Bétiques). *Geodinamica Acta*, 3, 107–116.
- Currás, J. and Torres-Ruiz, J. (1992) El skarn magnésico de magnetita-ludwigita del Cañuelo (Cordilleras Béticas occidentales). III Congreso Geológico de España. Salamanca. *Actas*, 3, 59–62.
- Dixon, R.H., Bangert, U., Harvey, A.J., and Kidd P. (1992) The use of Moiré contrast in the analysis of interfacial strain, 2, 701–702. *European Congress on Electron Microscopy*. Granada, Spain.
- Dowty, E. (1980) Crystal-chemical factors affecting the mobility of ions in minerals. *American Mineralogist*, 65, 174–182.
- Dutrow, B. and Norton, D. (1995) Evolution of fluid pressure and fracture propagation during contact metamorphism. *Journal of Metamorphic Geology*, 13, 677–686.
- Eggleton, R.A. and Banfield, J.F. (1985) The alteration of granitic biotite to chlorite. *American Mineralogist*, 70, 902–910.
- Etheridge, M.A., Wall, V.J., and Vernon, R.H. (1983) The role of the fluid phase during regional deformation and metamorphism. *Journal of Metamorphic Geology*, 1, 205–226.
- Etheridge, M.A., Wall, V.J., and Cox, S.F. (1984) High fluid pressures during regional metamorphism and deformation: Implications for mass transport and deformation mechanism. *Journal of Geophysical Research*, 89, B6, 4344–4358.
- Fisher, G.W. (1970) The application of ionic equilibria to metamorphic differentiation: An example. *Contribution to Mineralogy and Petrology*, 29, 91–103.
- (1973) Nonequilibrium thermodynamics as a model for diffusion-controlled metamorphic processes. *American Journal of Science*, 273, 897–924.
- (1977) Non equilibrium thermodynamics in metamorphism. In D.G. Fraser, Ed., *Thermodynamics in Geology*, p. 381–403. Reidel, Dordrecht.
- (1978) Rate laws in metamorphism. *Geochimica and Cosmochimica Acta*, 42, 1035–1050.
- Fisher, G.W. and Lasaga, A.C. (1981) Irreversible thermodynamics in Petrology. In *Mineralogical Society of America Reviews in Mineralogy*, 8, 171–210.
- Fortier, S.M. and Giletti, B.J. (1991) Volume self-diffusion of oxygen in biotite, muscovite and phlogopite micas. *Geochimica et Cosmochimica Acta*, 55, 1319–1330.
- Foster, C.T. (1981) A thermodynamic model of mineral segregations in the lower sillimanite zone near Rangeley, Maine. *American Mineralogist*, 66, 260–277.
- (1983) Thermodynamic models of biotite pseudomorphs after staurolite. *American Mineralogist*, 68, 389–397.
- (1986) Thermodynamic models of reactions involving garnet in a sillimanite/staurolite schist. *Mineralogical Magazine*, 50, 427–439.
- Fournier, R.O. and Potter, R.W. (1982) An equation correlating the solubility of quartz in water from 25° to 900° at pressures up to 10,000 bars. *Geochimica et Cosmochimica Acta*, 46, 1969–1973.
- García-Casco, A., Sánchez-Navas, A., and Torres-Roldán, R.L. (1993) Disequilibrium decomposition and breakdown of muscovite in high P-T gneisses, Betic alpine belt (southern Spain). *American Mineralogist*, 78, 158–177.
- García-Dueñas, V. and Balanyá, J.C. (1991) Fallas normales de bajo ángulo a gran escala en las Béticas occidentales. *Geogaceta*, 19, 33–37.
- Hartman, P. and Perdok, W.G. (1955) On the relations between structure and morphology of crystals. *Acta Crystallographica*, 8, 49–52.
- Holland, T.J.B. and Powell, R. (1990) An enlarged and updated internally consistent thermodynamic data set with uncertainties and correlations: the system K<sub>2</sub>O-Na<sub>2</sub>O-CaO-MgO-MnO-FeO-Fe<sub>2</sub>O<sub>3</sub>-Al<sub>2</sub>O<sub>3</sub>-TiO<sub>2</sub>-SiO<sub>2</sub>-C-H<sub>2</sub>-O<sub>2</sub>. *Journal of Metamorphic Geology*, 8, 89–124.
- Iijima, S. and Zhu, J. (1982) Electron microscopy of a muscovite-biotite interface. *American Mineralogist*, 67, 1195–1205.
- Joesten, R. (1977) Evolution of mineral assemblage zoning in diffusion metasomatism. *Geochimica et Cosmochimica Acta*, 41, 649–670.
- Kerrick, D.M. (1987) Fibrolite in contact aureoles of Donegal, Ireland. *American Mineralogist*, 72, 240–254.
- (1990) The Al<sub>2</sub>SiO<sub>5</sub> polymorphs. *Mineralogical Society of America Reviews in Mineralogy*, 22, 406 p.
- Kerrick, D.M., Lasaga, A.C., and Raeburn, S.P. (1991) Kinetics of heterogeneous reactions. In *Mineralogical Society of America Reviews in Mineralogy*, 26, 583–671.
- Kretz, R. (1983) Symbols for rock-forming minerals. *American Mineralogist*, 68, 277–279.
- Lasaga, A.C. (1981) Rate laws of chemical reactions. In *Mineralogical Society of America Reviews in Mineralogy*, 8, 1–68.
- (1986) Metamorphic reaction rate laws and development of isograds. *Mineralogical Magazine*, 50, 359–373.
- Loomis, T.P. (1972a) Contact Metamorphism of Pelitic Rocks by the Ronda Ultramafic Intrusion, Southern Spain. *Geological Society of America*, 83, 2449–2474.
- (1972b) Coexisting aluminum silicate phases in contact metamorphic aureoles. *American Journal of Science*, 272, 933–945.

Lundeen, M.T. (1978) Emplacement of the Ronda peridotite, Sierra Bermeja, Spain. Geological Society of America Bulletin, 89, 172–180.

Martín-Algarra, A. (1987) Evolución geológica alpina del contacto entre las Zonas Internas y las Zonas Externas de la Cordillera Bética (sector central y occidental). Thesis University of Granada. 1171 p.

Massonne, H.J. and Schreyer, W. (1987) Phengite geobarometry based on the limiting assemblage with potassium feldspar, phlogopite, and quartz. Contribution to Mineralogy and Petrology, 96, 212–224.

Mollat, H. (1968) Schichtenfolge un tektonischer Bau der Sierra Blanca und ihrer Umgebung (Betsische Kordilleren, Südsptanien). Geologisches Jahrbuch, 86, 471–521.

Nieto, F. and Sánchez-Navas, A. (1994) A comparative XRD and TEM study of the physical meaning of the white mica “crystallinity” index. European Journal of Mineralogy, 6, 611–621.

Nitkiewicz, A.M. (1989) The kinetics of the andalusite-sillimanite transformation. Transactions of American Geophysical Union, 70, 1392.

Obata, M. (1980) The ronda peridotite: Garnet-, spinel-, and plagioclase-lherzolite facies and the P-T trajectories of a high-temperature mantle intrusion. Journal of Petrology, 21, 533–572.

Price, N.S. and Cosgrove, J.W. (1990) Analysis of Geological Structures, 502 p. Cambridge University Press, New York.

Putnis, A. (1992) Introduction to Mineral Sciences, 457 p. Cambridge University Press, New York.

Ridley, J. (1985) The effect of reaction enthalpy on the progress of a metamorphic reaction. Advances in Physical Geochemistry, 4, 80–97.

Ridley, J. and Thompson, A.B. (1986) The role of mineral kinetics in the development of metamorphic microtextures. Advances in Physical Geochemistry, 5, 154–193.

Robin, P.-Y.F. (1979) Theory of metamorphic segregation and related processes. Geochimica et Cosmochimica Acta, 43, 1587–1600.

Rubie, D.C. (1986) The catalysis of mineral reactions by water and restrictions on the presence of aqueous fluid during metamorphism. Mineralogical Magazine, 50, 399–415.

Rubie, D.C. and Brearley, A.J. (1987) Metastable melting during the breakdown of muscovite + quartz at 1 kbar. Bulletin de Minéralogie, 110, 533–549.

Sánchez-Navas, A. and Galindo-Zaldívar, J. (1993) Alteration and deformation microstructures of biotite from plagioclase-rich dykes (Ronda Massif, S. Spain). European Journal of Mineralogy, 5, 245–256.

Schramke, J.A., Kerrick, D.M., and Lasaga, A.C. (1987) The reaction muscovite + quartz + andalusite + k-feldspar + water. Part 1. Growth kinetics and mechanism. American Journal of Science, 287, 517–559.

Shaw, D.M., Acosta, A., and Bea, F. (1996) Distribution of boron in serpentinization of the Ronda Peridotite. Geological Society of American Meeting, Abstracts, Vol., A-162.

Smyth, J.R. and Bish, D.L. (1988) Crystal Structures and Cation Sites of the Rock-Forming Minerals, 332 p. Allen and Unwin, Boston.

Spear, F. (1993) Metamorphic Phase Equilibria and Pressure-Temperature-Time Paths, 799 p. Mineralogical Society of America, Washington, D.C.

Strömgård, K.-E. (1973) Stress distribution during formation of boudinage and pressure shadows. Tectonophysics, 16, 215–248.

Thompson, A.B. and England, P.C. (1984) Pressure-temperature-time paths of regional metamorphisms. II. Their inference and interpretation using mineral assemblages in metamorphic rocks. Journal of Petrology, 25, 929–955.

Torres-Roldán, R.L. (1974) El metamorfismo progresivo y la evolución de la serie de facies en las metapelitas alpujarrides al S.E. de Sierra Almirajara (sector Central de las Cordilleras Béticas, S. de España). Cuadernos Geológicos, 5, 21–77.

— (1979) The tectonic subdivision of the Betic Zone (Betic Cordilleras, southern Spain): its significance and one possible geotectonic scenario for the westernmost Alpine belt. American Journal of Science, 279, 19–51.

— (1981) Plurifacial metamorphic evolution of the Sierra Bermeja peridotite aureole (southern Spain). Estudios Geológicos, 37, 115–133.

Tubía, J.M., Navarro-Vila, F., and Cuevas, J. (1986) High-temperature emplacement of the Los Reales peridotite nappe (Betic Cordillera, Spain). Journal of Structural Geology, 8, 473–482.

Veblen, D.R. (1992) Electron microscopy applied to nonstoichiometry, polysomatism, and replacement reaction in minerals. In Mineralogical Society of America Reviews in Mineralogy, 27, 181–229.

Veblen, D.R. and Ferry, J.M. (1983) A TEM study of the biotite-chlorite reaction and comparison with petrologic observations. American Mineralogist, 68, 1160–1168.

Vernon, R.H. (1987a) Oriented growth of sillimanite in andalusite, Placitas—Juan Tabo area, New Mexico, U.S.A. Canadian Journal of Earth Science, 24, 580–590.

— (1987b) Growth and concentration of fibrous sillimanite related to heterogeneous deformation in K-feldspar-sillimanite metapelites. Journal of Metamorphic Geology, 5, 51–68.

Vernon, R.H., Flood, R.H., and D’Arcy, W.F. (1987) Sillimanite and andalusite produced by base-cation leaching and contact metamorphism of felsic igneous rocks. Journal of Metamorphic Geology, 5, 439–450.

Walther, J.V. and Wood, B.J. (1984) Rate and mechanism in prograde metamorphism. Contribution to Mineralogy and Petrology, 88, 246–259.

Wintsch, R.P. and Andrews, M.S. (1988) Deformation induced growth of sillimanite: “stress” minerals revisited, Journal of Geology, 96, 143–161

Worden, R.H., Champness, P.E., and Droop, T.R. (1987) Transmission electron microscopy of the pyrometamorphic breakdown of phengite and chlorite. Mineralogical Magazine, 51, 107–121.

MANUSCRIPT RECEIVED JUNE 8, 1998  
 MANUSCRIPT ACCEPTED MAY 10, 1999  
 PAPER HANDLED BY ROBERT J. TRACY

## APPENDIX

### Rate law for diffusion-controlled model

Appendix Figure 1 shows the geometry of the muscovite crystal and of the core assemblage growing within it, where  $L$  is the edge of the square basal section of the muscovite host and  $X_C$  the thickness of the core, considered as equidimensional. The rate of the dissolution of muscovite per unit of area, through the heterogeneous reaction at the core-crystal host boundary,  $J_{Ms}^R$ , and the rate of K production per unit of area at this boundary,  $J_K^R$ , are proportional to their respective stoichiometric coefficients  $n_K^{(5)}$  and  $n_{Ms}^{(5)}$  in the observed reaction 5, so that

$$J_{Ms}^R = \frac{V_K^{(5)}}{V_{Ms}^{(5)}} J_K^R \quad (A1)$$

Because transport only occurs parallel to the mica layer due to the anisotropy of diffusion through the muscovite host, the equation for conservation of material would be

$$J_K^D S^D = J_K^R S^R; J_K^D 4X_C^2 = J_K^R 6X_C^2; J_K^R = \frac{2}{3} J_K^D \quad (A2)$$

where  $J_K^R$  is the K flux through the muscovite host,  $S^D$  is the diffusion surface, and  $S^R$  is the reaction surface at the core-crystal host boundary. The dissolution rate of muscovite in  $m^3/s$  is

$$\frac{dV_{Ms}}{dt} = J_{Ms}^R S^R V_{Ms} = J_{Ms}^R 6 X_C^2 V_{Ms} \quad (A3)$$

where  $v_{Ms}$  is the muscovite molar volume. For the geometry considered, it also holds that

$$\frac{dV_{Ms}}{dt} = \frac{dV_{Ms}}{dX_C} \frac{dX_C}{dt} = -3 X_C^2 \frac{dX_C}{dt} \quad (A4)$$

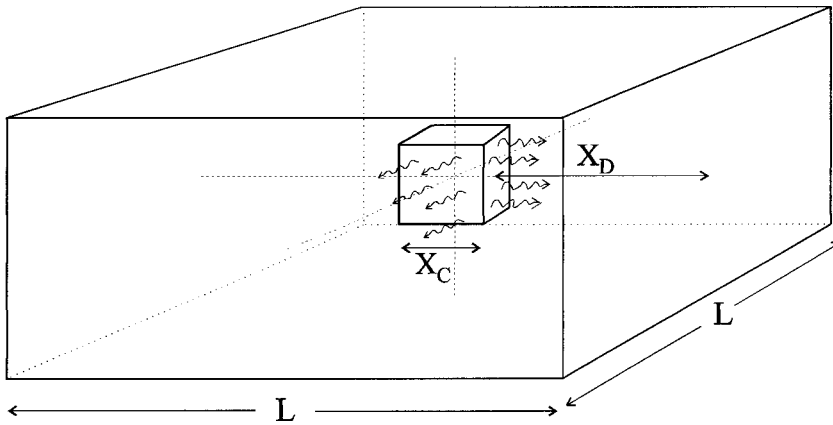
since  $V_{Ms} = V_{Ms}^0 - X_C^3$  where  $V_{Ms}^0$  is the initial volume of the muscovite crystal. Combining Equations A3, A4, A1, and A2 and rearranging them, then

$$-\frac{dX_C}{dt} = 2 J_{Ms}^R V_{Ms} = 2 \frac{V_K^{(5)}}{V_{Ms}^{(5)}} J_K^R V_{Ms} = 2 \frac{V_K^{(5)}}{V_{Ms}^{(5)}} \frac{2}{3} J_K^D V_{Ms}$$

Substitution of  $J_K^D = -L_{KK}^D \frac{\Delta\mu_K^{5-9}}{X_D}$ , where  $X_D$  is the length of the diffusion path, equals to  $1/2 (L - X_C)$ , gives

$$\frac{1}{2} (L - X_C) dX_C = \left( \frac{4}{3} \frac{V_K^{(5)}}{V_{Ms}^{(5)}} L_{KK}^D \Delta\mu_K^{5-9} v_{Ms} \right) dt$$

Integrating both sides of the equation and giving  $t$  as a function of  $X_C$ , we obtain



APPENDIX FIGURE 1. Geometry of muscovite and core used to obtain the rate law for the diffusion-controlled process.

$$t = \left( \frac{3}{8} L \frac{v_K^{(5)}}{v_{Ms}^{(5)}} \frac{1}{L_{KK}^D \Delta\mu_K^{5-9} v_{Ms}} \right) X_C - \left( \frac{3}{16} \frac{v_K^{(5)}}{v_{Ms}^{(5)}} \frac{1}{L_{KK}^D \Delta\mu_K^{5-9} v_{Ms}} \right) X_C^2 \quad (\text{A5})$$

#### Rate law for reaction-controlled model

In accordance with Lasaga (1986), we first need to determine the specific surface area of andalusite ( $\bar{A}$ ). Considering a cylindrical geometry (see Fig. 1A) for the andalusite growing in the muscovite crystal,

$$\bar{A} = \frac{2\pi r h}{\pi r^2 h} = \frac{2}{r} / \text{cm}$$

where  $r$  and  $h$  are the radius and height of the cylinder.

To determine the time for the texture formation, Equation 29 in Lasaga (1986) was used, for a  $P = 2$  kbar and  $T_{\text{eq}} = 601$  °C and an overstep of 5 °C, yielding a rate of  $1.9 \cdot 10^{-15}$  mols water/cm<sup>2</sup> andalusite/s. Since reaction 5 in this paper indicates a molar proportion between water and andalusite of 1:5/4, the reaction rate may be expressed as  $2.375 \cdot 10^{-15}$  moles andalusite/cm<sup>2</sup> andalusite/s. The total rate,  $R_t$ , is obtained by multiplying this rate,  $R$ , by

$$R_t = R \bar{A} = \frac{4.75 \cdot 10^{-15}}{r} \text{ mols / cm}^3 \cdot \text{s}$$

The number of andalusite moles per cm<sup>3</sup> is  $1.92 \cdot 10^{-2}$ , as one mole of andalusite occupies 52.20 cm<sup>3</sup>. Therefore, the time needed to form an andalusite crystal with a basal thickness of  $2r$  is given by

$$t = \frac{1.92 \cdot 10^{-2}}{4.75 \cdot 10^{-15}} = 4.03 \cdot 10^{12} r \text{ (in seconds)}$$

#### Diffusion-reaction boundary

To determine the kinetic mechanism governing metamorphic process studied here when thermodynamic and kinetic parameters are varied, rate laws were rewritten as a function of temperature overstep and diffusion coefficient  $L_{KK}^D$  (or intracrystalline porosity). So, in Equation A5, the consideration of  $L_{KK}^D$  and  $\Delta T$  as variables, and the substitution of  $\Delta\mu_K^{5-9} = \mu_K^5 - \mu_K^9 = \Delta G_{\text{Muscovite out}} + 1/4 \Delta G_{\text{Sill-And}}$  [where  $\Delta G_{\text{Muscovite out}} = -\Delta T \Delta S$  ( $\Delta S = 74.38 \text{ J/K}$ ) and  $\Delta G_{\text{Sill-And}} = -441.5 \text{ J}$  for the equilibrium condition at  $P = 2$  kbar], as well as making  $L$ ,  $v_K^{(5)}/v_{Ms}^{(5)}$ ,  $v_{Ms}$ , and  $X_C$  equal to 0.01 m, 1/2,  $1.428 \cdot 10^{-4} \text{ m}^3/\text{mol}$ , and 0.002 m, respectively, results in:

$$t = \frac{0.02363}{74.38 L_{KK}^D \Delta T + 110.375 L_{KK}^D}$$

where intracrystalline porosity,  $\phi$ , may be introduced easily, instead of  $L_{KK}^D$ , through Equation 16 of the text, which, for the case of  $P = 2$  kbar and  $T_{\text{eq}} = 600$  °C, is expressed by  $\phi = 7.2585 \cdot 10^9 L_{KK}^D$ .

In a similar way, reaction-control equation for  $P = 2$  kbar may be rewritten as function of  $\Delta T$ , so the curve representing the boundary between surface-control and diffusion-control will be given by:

$$\frac{3.05976 \times 10^{13}}{\Delta T^{2.69}} = \frac{0.02363}{74.38 L_{KK}^D \Delta T + 110.375 L_{KK}^D}$$